GEOLOGICAL SURVEY OF CANADA

OPEN FILE 2204

GEOLOGY OF THE HOWSE LAKE AREA, WESTERN LABRADOR

Jon M. Findlay
Tony D. Fowler
Tyson C. Birkett

1990

Energy, Mines and Resources Canada
Énergie, Mines et Ressources Canada
Canada

GEOLOGICAL SURVEY OF CANADA  COMMISSION GÉOLOGIQUE DU CANADA

OPEN FILE 2204

GEOLOGY OF THE HOWSE LAKE AREA, WESTERN LABRADOR[1]

Jon M. Findlay[2], Tony D. Fowler[2] and Tyson C. Birkett[3]

1 Contribution to the Canada-Newfoundland Mineral Development Agreement 1984-1989.

2 University of Ottawa, Department of Geology, Ottawa, Ontario, K1N 6N5.

3 Geological Survey of Canada, Québec Geoscience Center, P.O. Box 7500, Sainte-Foy, Québec, G1V 4C7.

Contribution to Canada-Newfoundland Mineral Development Agreement 1984-89, a subsidiary agreement under the Economic and Regional Development Agreement. Project funded by the Geological Survey of Canada

Contribution à l'Entente auxiliaire Canada/Terre-Neuve sur l'exploitation minérale 1984-89 faisant partie de l'Entente de développement économique et régional. Ce projet a été financé par la Commission géologique du Canada.


DEPARTMENT OF MINES
GOVERNMENT OF NEWFOUNDLAND AND LABRADOR


Energy, Mines and Resources Canada

Énergie, Mines et Ressources Canada

Canada

Abstract

Gabbroic sills of three major lithological types dominate the stratigraphy of the Howse Lake area of the central Labrador Trough. Normal sills show limited horizons of plagioclase-phyric gabbro, but are composed primarily of subophitic to ophitic hypersthene gabbro. Glomeroporphyritic sills consist predominantly of plagioclase-glomeroporphyritic hypersthene gabbro with minor intervals of non-glomeroporphyritic as well as anorthositic gabbro. The third sill type is characterized by relatively homogeneous, coarse grained anorthositic gabbro. Some sills represent multiple injection of melts, and field relationships suggest that the order of emplacement was normal sills- glomeroporphyritic sills- anorthositic sills. Glomeroporphyritic basalts of the Willbob Formation in the Doublet Terrane are texturally similar to sparsely glomeroporphyritic sills, and it is probable that they represent extrusive equivalents.

Geochemical variations among sill types indicate that they are comagmatic, and compositional differences have arisen from 1) variable crystal load in originally equivalent magma batches, and 2) *in situ* differentiation. *In situ* fractional crystallization has resulted in minor amounts of siliceous differentiates, and is thought to be the process by which rhythmic layering and sulphide enriched horizons were formed. Petrographic evidence indicates that plagioclase was a liquidus phase during sill emplacement and geochemical variation within sills suggests that fractionation of this mineral has controlled much of the local compositional variation. Isotopic evidence suggests that sulphur in sulphide enriched horizons and lenses has been derived in part from the host turbidites. Chalcophile element concentrations, including the Platinum Group Elements, are generally low.

Table of Contents

Abstract i

Chapter 1: Introduction

1.1 Purpose and Scope 1
1.2 Location, Access, Physiography 1
1.3 Previous Work 1
1.4 Acknowledgements 3

Chapter 2: General Geology

2.1 Regional Setting 4
2.2 Local Geology 6
2.3 Age Relationships 8

Chapter 3: Lithological Descriptions

3.1 Le Fer Formation 10
3.2 Wakuach Gabbro 13
3.2.1 General Lithological Descriptions 13
3.2.2 Petrography 17

Chapter 4: Metamorphism

4.1 Le Fer Formation 20
4.2 Wakuach Gabbro 20

Chapter 5: Geochemistry

5.1 Basalt Geochemistry 21
5.2 Gabbro Geochemistry 25

Chapter 6: Petrogenesis
6.1 Le Fer Formation 30
6.2 Wakuach Gabbro 31

Chapter 7: Economic Geology

7.1 Sulphide Occurrences 33
7.2 Sulphur Isotopes 34
7.3 Platinum Group Element Potential 37

References 40

Appendix A: Assay Results 43

Appendix B: Sample Descriptions 48

Appendix C: Rare Earth Element Analyses 56

Appendix D: Whole Rock Analyses 57

1:20,000 Scale Geological Map, Howse Lake, Labrador ... pocket

Chapter 1: Introduction

1.1 Purpose and Scope

Gabbroic sills dominate the stratigraphy of the Howse Lake area, located approximately 40 kilometers northeast of Schefferville, Québec, in the central portion of the Lower Proterozoic Labrador Trough (Figure 1). Similar sills in the Wakuach Lake area of the central Trough have been subdivided into three lithological types which were considered comagmatic (Baragar, 1960; 1967). The present study was initiated to examine the *in situ* differentiation of the Howse Lake sills, to determine the petrogenetic relationship between different sill types, to establish the origin of plagioclase glomerocrysts, and to evaluate the economic potential of sulphide mineralization hosted by the intrusions. As part of a regional examination of western Labrador metallogeny, the area was mapped during the field seasons of 1985 and 1986, and detailed sample traverses were conducted across suitable exposures during the 1986 and 1987 seasons. This work forms part of the ongoing Ph.D. thesis of JMF, and hence represents preliminary interpretations of data collected during the course of the study.

1.2 Location, Access, Physiography

The map area covers approximately 80 square kilometers in the vicinity of Howse Lake, Labrador (NTS map sheets 23-O/2 E and 23-O/1 W). Due to the isolated nature of the location, access is restricted to float equipped aircraft or helicopters, with Schefferville providing the nearest operational base. Gabbroic sills form low, rounded ridges separated by narrow, elongate lakes or marshes commonly developed on the less resistant host rock strata. Exposure is generally poor except near the southern end of Howse Lake where semi-continuous outcrop permitted detailed sampling of the intrusive rocks at several locations.

1.3 Previous Work

The stratigraphy, structure and evolution of the Labrador Trough have been summarized by Frarey and Duffell (1964), Dimroth (1970; 1978), Baragar and Scoates (1981), Wardle and Bailey (1981) Wardle (1982), Hoffman (1987) and Wardle et al (in press). The petrology of the tholeiitic rocks has been discussed in detail by Baragar (1960; 1967) and Frarey (1967).

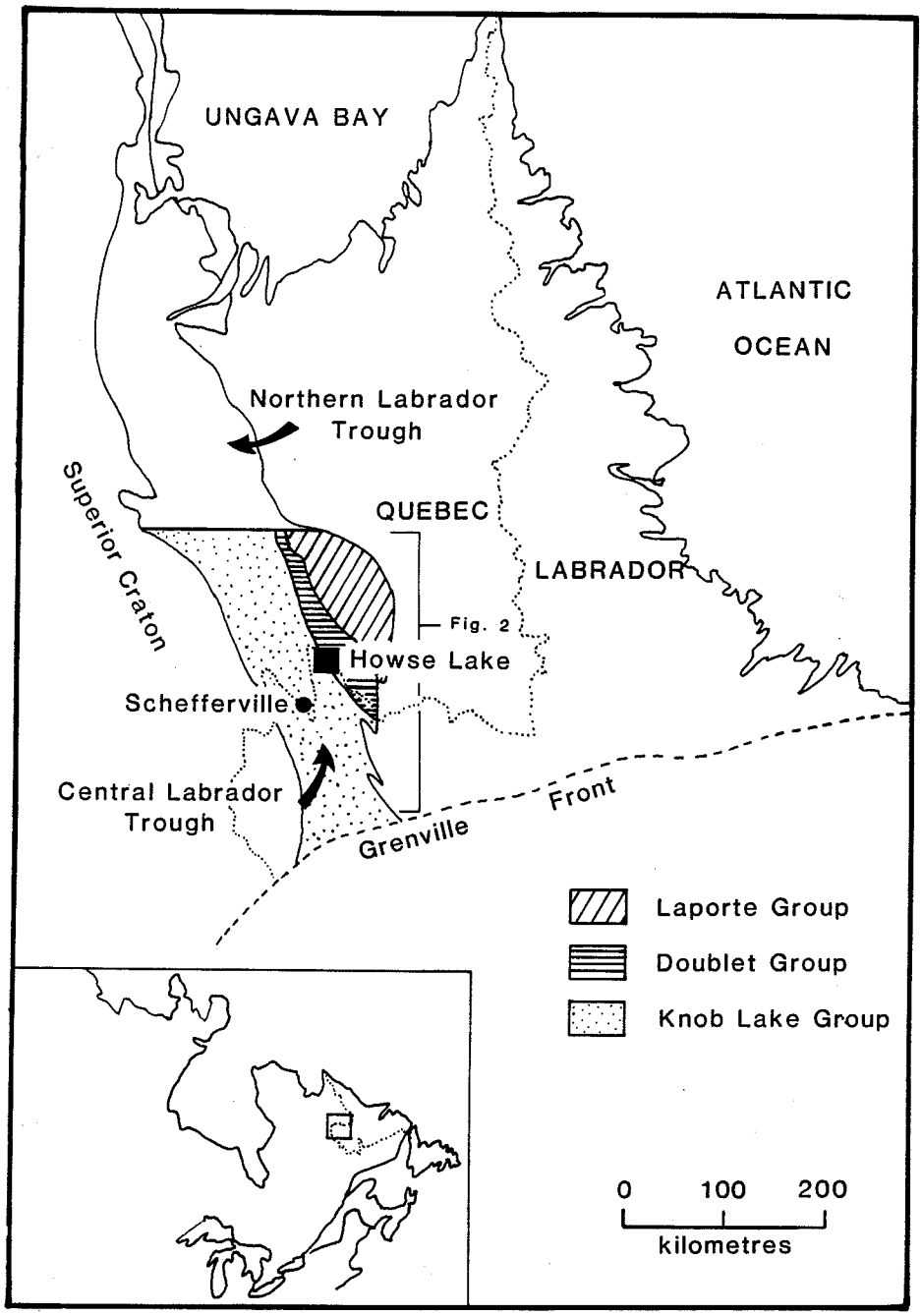

Figure 1. Location of the Howse Lake area and distribution of the principal stratigraphic units of the Central Labrador Trough. After Wardle and Bailey (1981). Location of Figure 2 is indicated.

One inch to one mile scale mapping covering the Howse Lake area was completed by the Geological Survey of Canada (Frarey, 1967).

The Labrador Trough has been the site of ongoing mineral exploration since the discovery of iron ore at Sawyer Lake in 1937. The Labrador Mining and Exploration Company and the Hollinger-North Shore Exploration Company Ltd. have been responsible for much of this work. Numerous base metal sulphide showings have been discovered, but none have proven economic. Re-evaluation of sulphide showings for their Platinum Group Element (PGE) and gold contents has been conducted by numerous companies since 1985. Renewed interest on the part of industry in the mineral potential of specific geologic environments has led to a significant increase in the amount of research being carried out in the Labrador Trough, and this will provide a better basis for interpretation of the geological setting of the area.

1.4 Acknowledgements

This study is a contribution to the evaluation of the mineral resource potential of western Labrador under the Canada-Newfoundland Mineral Development Agreement. La Fosse Platinum Group Inc. provided logistic support and work leave (to JMF) during the field season of 1987. Canaustra Gold Exploration Ltd. provided additional financial support for analytical work. The expertise and assistance of Dan Richardson, Don Watanabe, Mike Regular, Sylvie Caza, Ann Lesage and Jacques Wortman are gratefully acknowledged. The paper has benefited from the comments and suggestions of W.R.A. Baragar, who reviewed the manuscript.

Chapter 2: General Geology

1.1 Regional Setting

The Labrador Trough is a linear belt of Lower Proterozoic (Aphebian) igneous and sedimentary rocks which extends for approximately 1000 km from Ungava Bay to Wabush/Labrador City in northeastern Québec and western Labrador (Figure 1). The central portion of the Trough comprises three principal stratigraphic units which have been subdivided into four lithotectonic regions by Wardle et al (in press). On the basis of mapping and geochronological work in the Howse Lake area, we suggest that the four-fold subdivision be revised to recognize a structural and lithological break within the Howse Zone of Wardle et al, which delimits the western occurrence of glomeroporphyritic gabbro. We reserve the term Howse Zone for the area between the Walsh Lake - Connolly Lake Fault to the east and the limit of glomeroporphyritic gabbro to the west. For the area bounded by the limit of glomeroporphyritic gabbro and the Ferrum River Fault we introduce the term Ferrum Zone (Figure 2). The dominantly northwest-southeast structural trend within the belt has resulted from compressive deformation accompanying Hudsonian orogenesis.

In the westernmost subdivision, the Schefferville Zone, Archean basement of the Superior Craton (Ashuanipi Metamorphic Complex) is unconformably overlain by members of the Knob Lake Group (Figure 3), a repeated sequence of shallow water clastic and chemical sedimentary rocks grading to deeper water turbidites, with minor amounts of intercalated alkaline volcanic rocks. In contrast, Knob Lake strata in the Ferrum and Howse Zones consist largely of deep water sediments and voluminous mafic igneous rocks. The Schefferville and Howse Zones of Wardle et al (in press) are delineated by east-dipping thrust faults, and a similar break is postulated between the Howse and Ferrum Zones.

The Doublet Group, a thick sequence of predominantly mafic volcanic and pyroclastic rocks, with relatively minor amounts of black slate, quartzite and metagreywacke (Baragar, 1967; Frarey, 1967) occupies the central portion of the central Trough (Doublet Terrane). This sequence is generally in tectonic contact with the Knob Lake Group along the Walsh Lake-Connolly Lake Fault (Frarey, 1967; Wardle and Bailey, 1981). However, a conformable relationship between the Doublet Group and underlying Knob Lake sediments was reported in the Ahr Lake area by Baragar (1958). The Laporte Group, an assemblage of quartz-feldspar-biotite schist, garnet-staurolite-mica schist, tremolite-actinolite rock and amphibolite (Baragar, 1967; Frarey, 1967) constitutes the easternmost subdivision of the central Trough (Laporte Terrane). The Laporte Group, interpreted as a metamorphosed succession of clastic sedimentary and volcanic rocks intruded

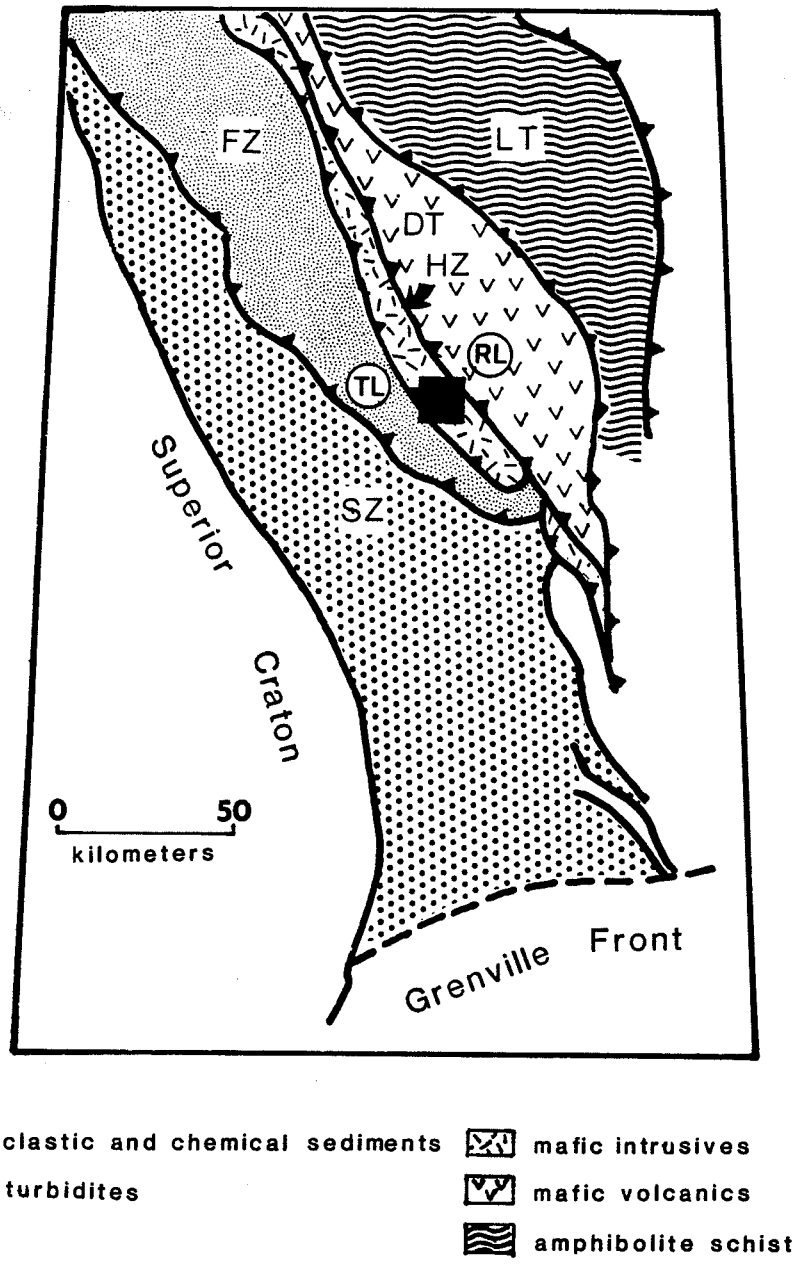

Figure 2. Lithotectonic subdivision of the Central Labrador Trough. SZ = Schefferville Zone, FZ = Ferrum Zone, HZ = Howse Zone, DT = Doublet Terrane, LT = Laporte Terrane. Location of the study area is denoted by the filled square. Tait Lake (TL) and Retty Lake (RL) sample locations are indicated by circles. Modified after Wardle et al (1988).

by mafic and ultramafic plutonic rocks (Baragar, 1967), has been thrust westward over the Doublet Group (Wardle and Bailey, 1981). Metamorphic grade increases eastward from sub-greenschist in the Knob Lake Group, to greenschist in the Doublet Group, and reaches amphibolite facies in the Laporte Group.

The stratigraphic sections of the Ferrum Zone, Howse Zones and the Doublet Terrane have been substantially thickened by a profusion of mafic (Wakuach Gabbro) and ultramafic (Retty Peridotite) sills of the pre-orogenic Montagnais Group. As noted previously, the mafic intrusions have been subdivided by Baragar (1960) into three lithological types: normal gabbro, plagioclase-glomerophyric gabbro (blotchy gabbro, leopard rock) and metagabbro. Baragar (1960) considered metagabbro (Doublet Terrane) to be the metamorphosed equivalent of normal gabbro (Ferrum and Howse Zones), and attributed mineralogical and geochemical differences between the two lithologies to the abrupt increase in metamorphic grade across the Walsh Lake-Connolly Lake Fault. Spectacular glomeroporphyritic texture is best developed in sills of the Howse Zone, but is also present locally in a thick sequence of the tholeiitic pillow basalts of the Willbob Formation, which caps the Doublet Group. Basaltic and gabbroic rocks of the Ferrum and Howse Zones and the Doublet Terrane have been considered comagmatic (Baragar, 1960; Wardle and Bailey, 1981), and together constitute a major igneous suite of tholeiitic affinity. The relationship between the tholeiitic suite, and the Retty Peridotite and metamorphosed volcanic and plutonic rocks of the Laporte Group, has not been determined.

1.2 Local Geology

Mafic sills constitute 75% of the stratigraphic section at Howse Lake, occurring as thin conformable bodies of substantial strike lengths. Bedrock exposure is poor except near the southern end of Howse Lake where semi-continuous outcrop permitted detailed sampling of the various lithologies (Figure 4 and accompanying map). Gabbroic melts were emplaced within a sequence of turbidites containing thin horizons of volcaniclastic, pyroclastic and mafic volcanic rocks, all of which are preserved as narrow and discontinuous wedges between sills. In general, the distribution of rock units in the map area conforms to the regional pattern of northwesterly trending structures prevalent in the Labrador Trough. Lithological contacts, bedding in sedimentary units and layering in intrusive rocks consistently show northwesterly strikes and moderate to steep northeasterly dips. Cross- and graded-bedding in turbidites and volcaniclastic horizons indicate a northeasterly younging direction.

Rocks in the study area have suffered little deformation during Hudsonian orogenesis. The only obvious manifestation of

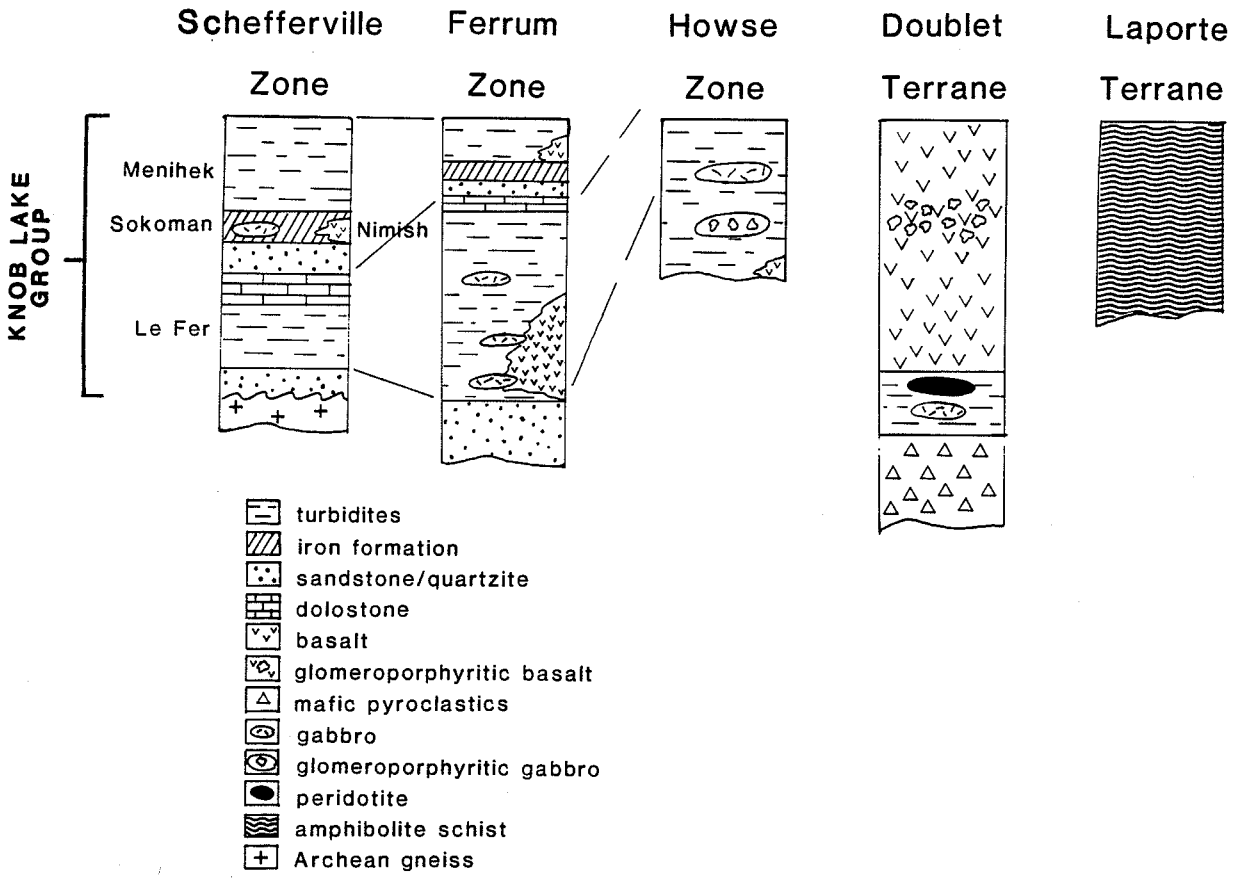

Figure 3. Generalized stratigraphic sequence in the Schefferville, Ferrum and Howse Zones, and Doublet Terrane.

imposed stress occurs in the tight folding and cleavage development locally evident in Le Fer turbidites. Folding is generally confined to strata adjacent to sill contacts, and may be related to drag stresses during magma emplacement. No major faulting is exposed, although stratigraphic relations suggest that the western limit of glomeroporphyritic gabbro near Attikamagen Lake is in fact a fault controlled boundary.

1.3 Age Relationships

The age of formation of the supracrustal suite which comprises the central Labrador Trough is constrained by dates of 2670-2650 Ma for the Ashuanipi Metamorphic complex (Percival and Girard, 1988) which forms the western basement, and approximately 1750 Ma for Hudsonian orogenesis (Fryer, 1972) A sample from a glomeroporphyritic gabbro sill at Howse Lake provided a concordant U-Pb zircon date of 1883.8 +1.6, -1.5 Ma and syenitic cobbles in conglomerate interbedded with alkali basalts of the Nimish Formation produced an indistinguishable U-Pb zircon date of 1879 +5.2, -3.5 Ma (Findlay et al, in preparation). The cobbles and alkali basalts show similar geochemical characteristics and are considered comagmatic. The Nimish conglomerates contain cobbles of cherty iron formation and the suite is aerially restricted, interfingering with the Sokoman Iron Formation at the limits of its occurrence. The Nimish suite has been interpreted as local, rift-related volcanic activity which interrupted the otherwise quiescent deposition of banded iron formation (Evans, 1978). Since conglomerates and flows are interbedded, the conglomerates, basalts and iron formation are approximately coeval. Consequently, crystallization of gabbroic sills at Howse Lake was essentially contemporaneous with development of the Nimish Formation, and the host rocks to the sills must therefore predate the Nimish and Sokoman Formations. Previous mapping has assigned the turbidite sequence of the Howse Zone to the Menihek Formation. On the basis of the zircon dates and stratigraphic relations, we suggest a correlation with the Le Fer Formation. Wardle et al (in press) suggest that a U-Pb zircon date of 2142 +4,-2 reported for rhyolite interbedded with basaltic rocks from the north-central Trough (Clarke, 1984) is the approximate age of Le Fer volcanism. On the basis of textural and geochemical similarities, Baragar (1960) and others have suggested that the Wakuach Gabbro and Willbob Formation are comagmatic.

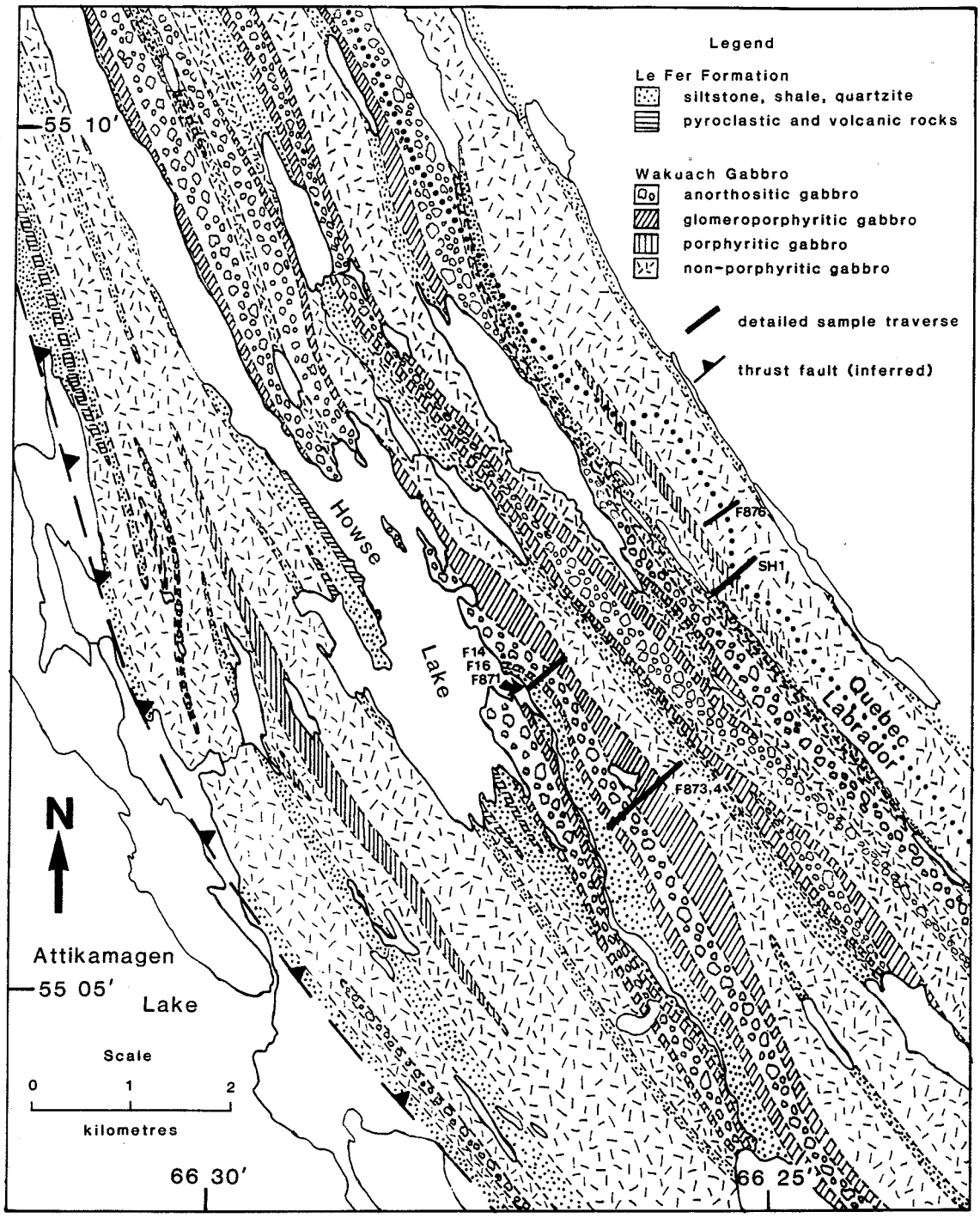

Figure 4. Generalized distribution of rock types in the Howse Lake area, and locations of detailed sample traverses.

Chapter 3: Lithological Descriptions

3.1 Le Fer Formation

The host rock succession is dominated by an immature sequence of slightly metamorphosed greywacke, siltstone and shale, with minor intervals of volcaniclastic rocks and mafic flows. The sequence is poorly exposed and the relative erosional resistance of sills and host rocks has resulted in a ridge-valley topography in which the host rocks underlie elongate lakes and marshes. Poor exposure prevents estimation of the relative proportions of individual lithologies.

Turbidite Sequence

Most exposures of the sedimentary units are well stratified and in many locations cross- and graded-bedding are preserved. Greywacke and siltstone, differentiated on the amount of fine grained matrix, are the predominant rock types in the succession and are interlaminated on a scale of centimeters. In both lithologies the coarser detrital component consists principally of angular to subrounded grains of quartz, plagioclase and alkali feldspar, and the relative proportions of these phases is highly variable. Less frequently, angular to rounded fragments of basaltic and granitic rocks, jasper or carbonates are the dominant clastic components and define lithic greywacke horizons. Sphene is a common component of both greywacke and siltstone, and magnetite, ilmenite, rutile and zircon are ubiquitous accessory constituents. Biotite occurs as fine grained, prismatic to highly irregular crystals intergrown with feldspar and quartz, and is locally abundant in finer grained lithologies. Chlorite forms minute flakes between coarser detritus, and is intergrown with clay minerals and carbonate in fine grained matrices. Some samples show laminations containing concentrations of finely disseminated pyrite and pyrrhotite. Minor chalcopyrite is occasionally associated with the iron sulphides.

Shales range from grey to black in colour and consist largely of a cryptocrystalline intergrowth of clay minerals and slightly coarser chlorite enclosing quartz and feldspar grains. Exposures may be well laminated or massive, and locally show a marked fissility. Fractures are filled by quartz, carbonate, pumpellyite or chlorite and often contain secondary pyrrhotite or pyrite. Both sulphide phases may be present as fine disseminations, and pyrite locally forms up to 1 centimeter thick laminae and lenses, or coarse blebs. Arkosic laminae and lenses (Figure 5A) consist largely of angular to subrounded, fine to medium sized grains of alkali

feldspar, quartz and plagioclase, with minor interstitial biotite and chlorite flakes. As in siltstones, sphene, rutile, zircon, magnetite-ilmenite, pyrite and pyrrhotite are common accessory phases.

Pyroclastic and Volcanic Rocks

Pyroclastic rocks were observed in a single horizon along the western shoreline of Howse Lake where they are interbedded with volcanic and volcaniclastic rocks. At this location, the pyroclastic unit consists of lapilli tuff (IUGS classification; Schmid, 1981) in which angular fragments of mafic volcanic rock and vitric shards are set in a chloritic-tuffaceous matrix. There is an apparent up-section gradation from lithologies in which the mean diameter of pyroclasts is approximately 2cm (Figure 5B), to varieties that are principally composed of 2 to 8 mm sized vitric shards (Figure 5C). The pyroclastic lithologies are overlain by graded beds of reworked volcaniclastic sediments which contain volcanic fragments, vitric shards and poorly sorted epiclastic material including jasper, set in a cryptocrystalline matrix of chlorite, clays and carbonate (Figure 5D).

Volcanic rocks occur in thin horizons interbedded with turbidites or pyroclastic rocks in the western half of the map area. The flows are basaltic, fine grained, dark green to grey on fresh surfaces, and may be pillowed, amygdaloidal or massive. Petrographically, the basalts show a decussate fabric in which plagioclase forms prismatic laths intergrown with prismatic to acicular Fe-Ti oxides and equant to irregularly shaped clinopyroxene. Clinopyroxene is commonly completely pseudomorphed by actinolite or chlorite, and plagioclase shows moderate to strong replacement by clinozoisite or albite. Magnetite occupies 5-15% of the samples as acicular to skeletal grains showing random orientations. An unusual feature is the abundance of sphene, which constitutes up to 15% of some samples as prismatic, diamond shaped or irregular grains which are generally partially to completely replaced by fine grained leucoxene. Apatite forms small granular crystals between plagioclase laths and carbonate may occur as irregular interstitial crystals. Minor pyrite or pyrrhotite is generally present as disseminated grains or secondary blebs. Amygdules are filled by fibrous chlorite, fine grained fan shaped aggregates of pumpellyite or, less commonly, calcite.

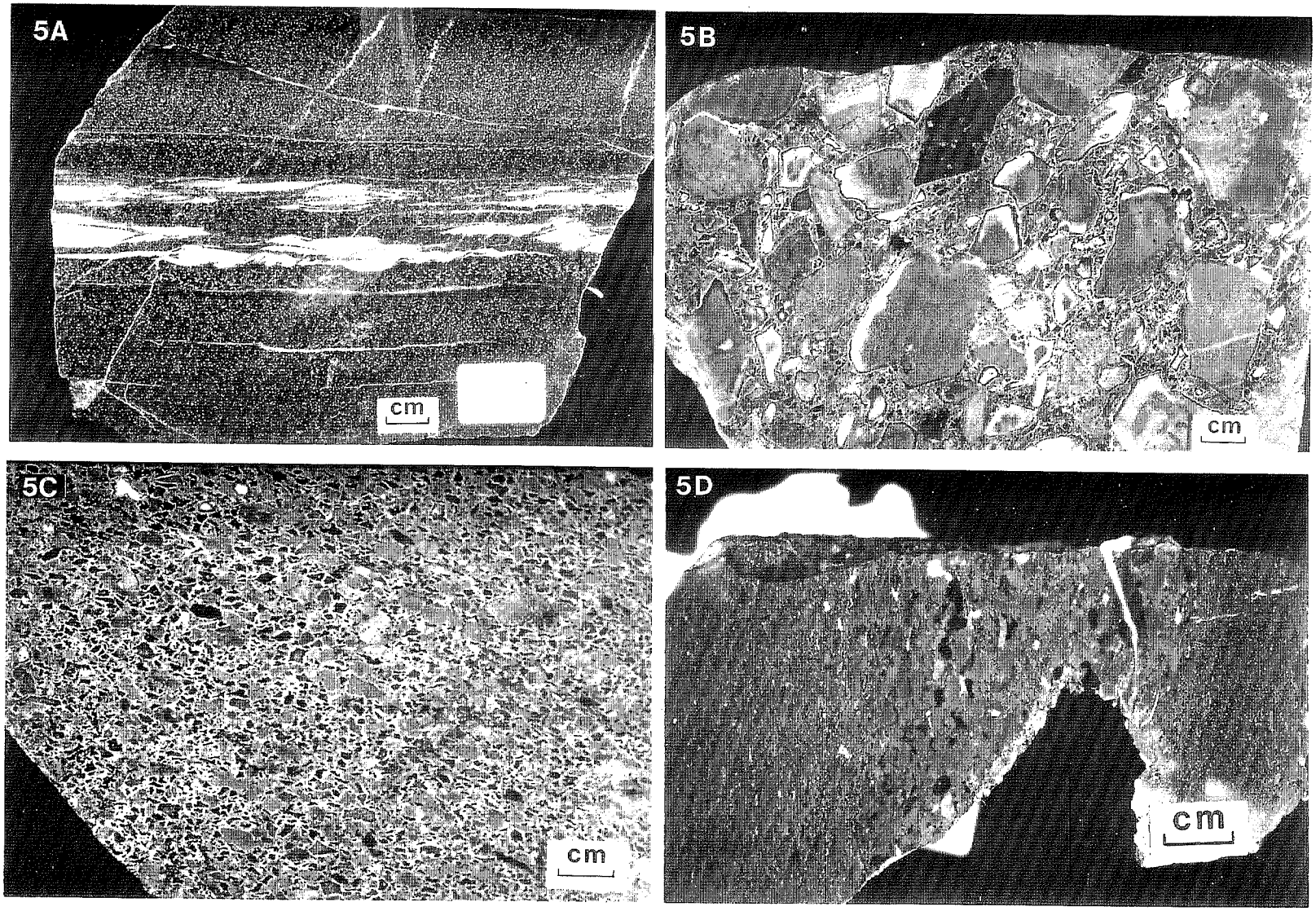

Figure 5. (A) Arkosic laminae in siltstone. Note speckled appearance resulting from metamorphic recrystallization.
(B) Pyroclastic horizon in which large volcanic clasts dominate.
(C) Pyroclastic horizon in which vitric shards dominate.
(D) Volcaniclastic interval in which volcanic and sedimentary clasts occur in graded beds.

3.2 Wakuach Gabbro

Gabbroic sills of the Howse Lake area range from 300 to 1000 meters in thickness, and may show significant variation in thickness along strike. Sills are conformable to the host rock sequence, and generally strike northwesterly and dip 50-75° to the west. The occurrence of plagioclase phenocrysts and glomerocrysts, and their size and frequency distribution, give rise to the most obvious lithological variations among and within sills. A three-fold classification is used in this report to distinguish the major sill types. Normal gabbro (Baragar, 1960) is retained to denote intrusions of a predominantly non-porphyritic nature. Glomeroporphyritic gabbro sills are those in which plagioclase aggregates occur in variable proportions throughout much of the intrusion. The third subdivision, anorthositic gabbro, is characterized by coarse grain size and plagioclase contents ranging from 60-85% of the rock.

3.2.1 General Lithological Descriptions

Glomeroporphyritic Gabbro

Most sills which exhibit well developed glomeroporphyritic texture have marginal zones of non-porphyritic to sparsely porphyritic-glomeroporphyritic gabbro (Figure 6A), which range in thickness from 5m to 100m. The size and frequency of feldspar glomerocrysts increase gradationally toward the central part of these sills, producing a gabbroic phase that is regularly spotted with 1 to 5 centimeter sized plagioclase aggregates (Figure 6B). Bands of coarse grained anorthositic gabbro are present in many of the glomeroporphyritic sills of the area, and sharp intrusive contacts indicate that these represent later magmatic injections. A core phase, in which large glomerocrysts are set in a matrix of medium to coarse grained subophitic gabbro is erratically developed within some sills (Figure 6C). Aggregates may reach 18 centimeters in diameter and form what is essentially a close-packed framework with relatively minor amounts of interstitial groundmass. The core phase generally shows sharp undulating contacts with enclosing glomeroporphyritic gabbro (Figure 6D). A related lithology, in which smaller aggregates are close packed in thin bands or lenses, is locally present (Figure 7A).

Magmatic phase layering, consisting of alternating plagioclase- and clinopyroxene-rich layers, 1-2 cm in thickness (Figure 7B), is present in the marginal zones of several sills. Layering is prominent in outcrop as a result of differential weathering, but is poorly defined in thin

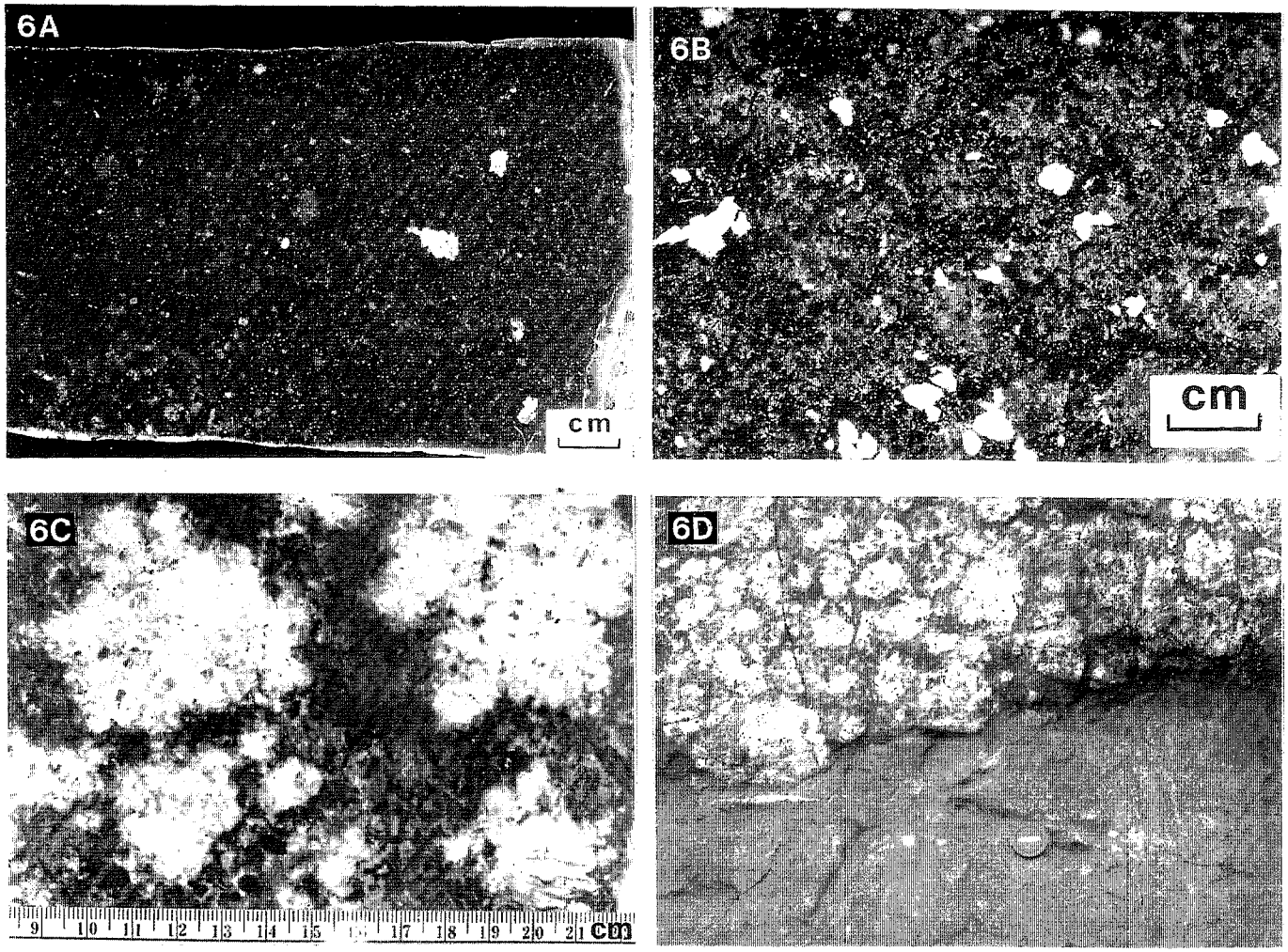

Figure 6. (A) Infrequent and small glomerocrysts in chilled gabbro adjacent to sill contact.
(B) Ophitic bronzite gabbro containing abundant glomerocrysts.
(C) Large plagioclase aggregates in medium grained gabbro characterize the core phase locally developed in some sills.
(D) Core phase in sharp contact with enclosing sparsely glomeroporphyritic gabbro.

section. A conspicuous feature of glomeroporphyritic lithologies is the occurrence of felsic veins or bleached zones in which a fine grained assemblage of quartz, epidote, chlorite, albite and uralitic amphibole replaces the original gabbroic minerals (Figure 7C). These zones range in thickness from 1 cm to 1 m, may be crosscutting or conformable, and appear to have developed through the passage of a volatile enriched phase, possibly a water saturated magmatic fluid.

Normal Gabbro

Normal gabbro sills consist predominantly of monotonous, medium grained, subophitic to ophitic gabbro, which may be chilled to fine grained basaltic material at contacts. All normal sills examined in the study area contain horizons of glomeroporphyritic or porphyritic gabbro in which centimeter-sized plagioclase aggregates and smaller phenocrysts form up to 10% of the rock. The intervals occupy variable proportions of the total sill thickness. Irregularly-shaped areas of pegmatitic gabbro are present in the upper parts of some sills. These are mineralogically similar to, and grade into, the enclosing medium grained gabbro, and may reflect localized volatile concentration. Felsic veins, identical to those found in glomeroporphyritic sills, are locally developed.

Anorthositic Gabbro

Anorthositic gabbro occurs as distinct sills and as sharply delineated bands within glomeroporphyritic sills. Similar bands were not observed in normal gabbro sills. The predominant texture is one of medium to coarse grained subophitic to ophitic gabbro in which the grain size of groundmass and glomerocryst plagioclase crystals are similar, and the two populations of feldspar are almost indistinguishable. Where anorthositic gabbro occurs within a glomeroporphyritic sill, the contact is sharp and the earlier gabbro often shows disruption and veining adjacent to the contact (Figure 7D). Anorthositic gabbro forming distinct, individual sills may show basaltic chilled margins similar to the other sill types. The size and abundance of aggregates increases quickly moving away from sill contacts, and the coarse grained anorthositic lithology is developed within 30-50 m. Anorthositic gabbro contains rare enclaves of non-porphyritic gabbro.

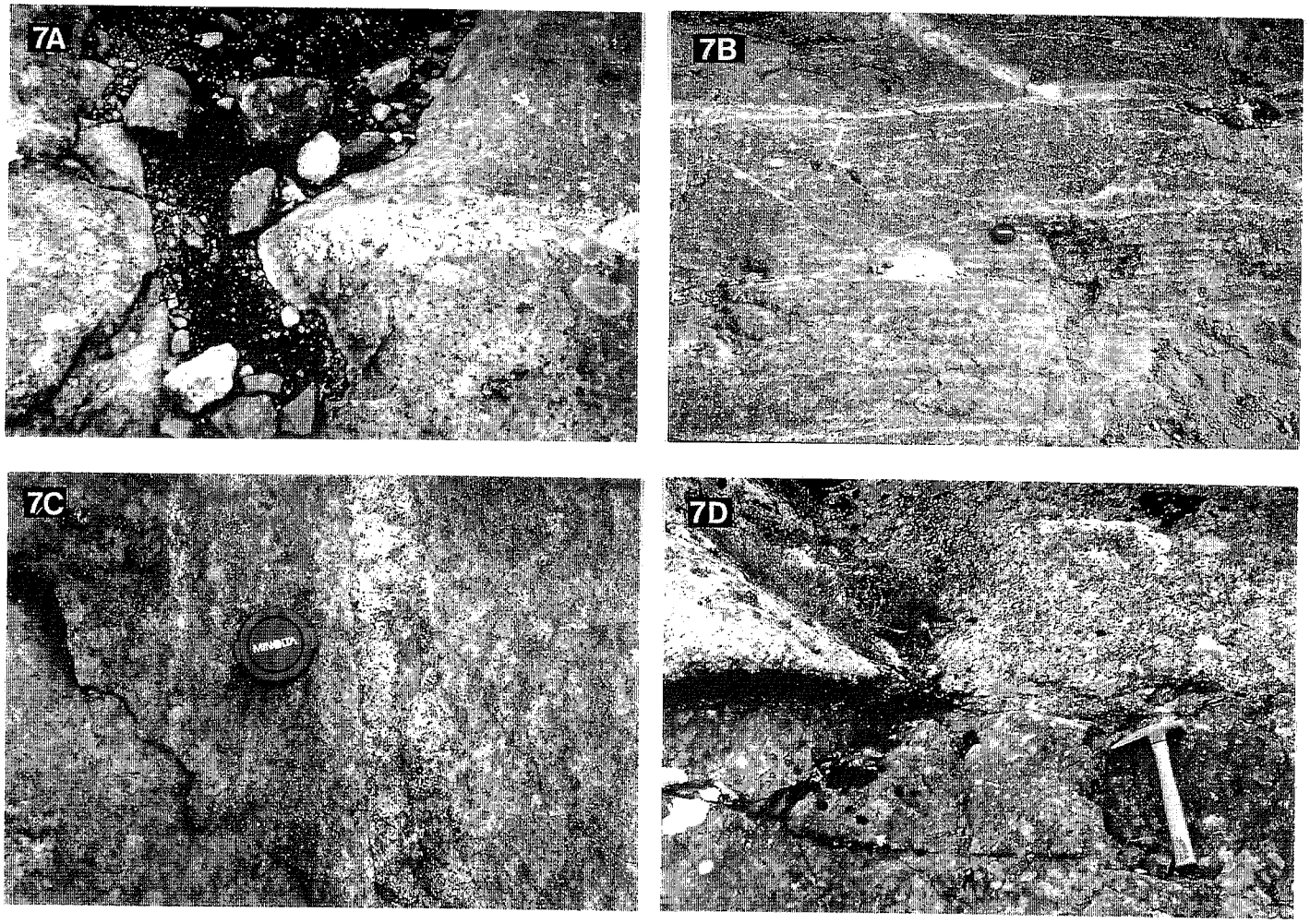

Figure 7. (A) Flow feature in glomeroporphyritic gabbro in which plagioclase aggregates are concentrated in a thin discontinuous lens.
(B) Alternating plagioclase- and clinopyroxene-rich layers in sparsely glomeroporphyritic gabbro.
(C) Felsic vein in sparsely glomeroporphyritic gabbro.
(D) Intrusive contact between anorthositic gabbro and underlying glomeroporphyritic gabbro. Note disruption of the latter at the contact.

3.2.2 Petrography

Gabbroic Matrices

The matrices of the two sills studied in detail show similar petrographic variation across their thicknesses (Figure 8). The lower contacts are marked by fine grained gabbro in which decussate, randomly arranged plagioclase laths are intergrown with anhedral, equant to angular, intergranular augite grains. Minor orthopyroxene may be present as anhedral grains, and alkali feldspar forms minor intergranular material. Sphene, magnetite and pyrrhotite are common accessory phases. Grain size increases away from the chill zone and sub-ophitic to ophitic texture develops with coarse augite grains enclosing plagioclase. Orthopyroxene increases in mode across the central parts of the sills, initially forming anhedral to subhedral tabular grains, then occurring as coarse irregular grains enclosing plagioclase. The textural change in orthopyroxene is accompanied by a decline in the augite content, and by the increasingly granular nature of the latter grains. The upper portions of the sections show a return to the subophitic to ophitic gabbro in which orthopyroxene is a minor phase. In both sills this portion contains moderately abundant intergranular alkali feldspar, and granophyric intergrowths of alkali feldspar and quartz are locally present. In one sill, the highest exposed level contains a horizon in which magnetite forms equant cumulus grains which comprise 15% of the rock. With the exception of the intrusive contact with anorthositic gabbro, mineralogical and textural variation in the sections are gradational. No extreme felsic differentiates are present in either section, although regional mapping indicates quartz gabbro and quartz monzogabbro are locally developed.

In terms of mineralogy, anorthositic gabbro is similar to the matrices of normal and glomeroporphyritic gabbro, but contains significantly greater plagioclase content. Glomerocrysts generally occupy 50% of the rock, with coarse clinopyroxene, orthopyroxene and oxides filling interstices. Groundmass plagioclase ranges from medium grained individual crystals enclosed by pyroxene, to coarser laths adjoining glomerocrysts. Pyrrhotite and lesser chalcopyrite may occur as coarse interstitial grains. Samples commonly show abundant, very fine, chlorite-filled fractures, and primary minerals usually show greater alteration than in the medium grained matrices of glomeroporphyritic or normal gabbro.

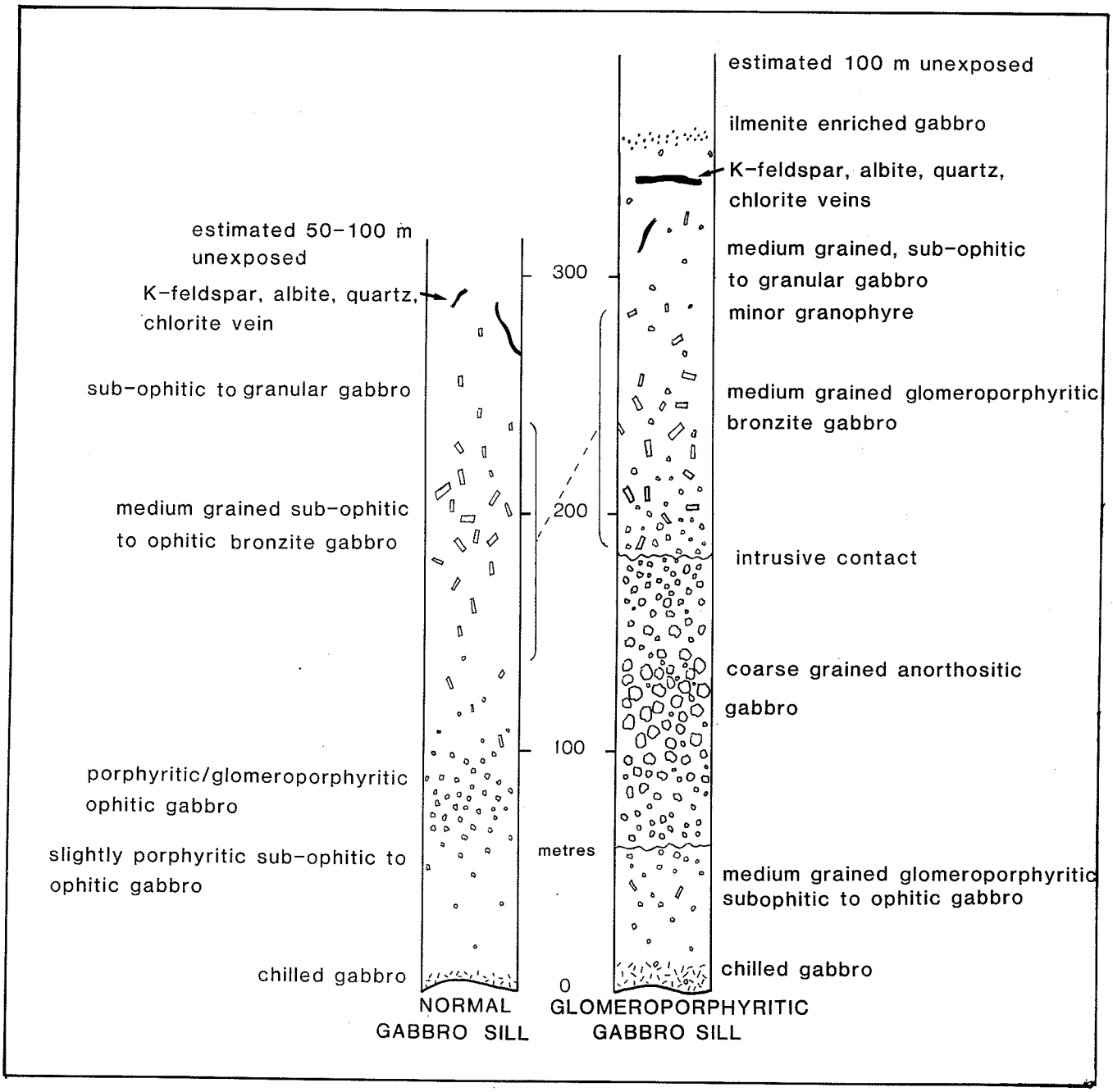

Figure 8. Schematic illustration of the lithological variation exhibited by the normal and glomeroporphyritic gabbro sills.

Glomerocrysts

Glomerocrysts are crudely spherical to irregularly shaped plagioclase aggregates with low ferromagnesian mineral contents, usually less than 5%. Individual crystals are subhedral and blocky and often show strong oscillatory zonation. Aggregates may consist of from three to more than thirty interlocking crystals, commonly adjoining at triple point junctions. Interstices are occupied by more sodic overgrowths on plagioclase primocrysts, or by clinopyroxene, hornblende or magnetite. The size of aggregates is dependent both on the size of individual crystals and the total number of crystals present, and large aggregates are most commonly observed in coarse grained matrices. Differences in crystal morphology, size and degree of alteration between matrix and glomerocryst feldspar indicate that two distinct crystal populations are represented. Preliminary electron microprobe determinations of plagioclase compositions indicate that glomerocryst cores (An_{75-85}) are generally more calcic than the cores of groundmass crystals (An_{55-75}). Microprobe work aimed at quantifying differences in composition and zonation between the two crystal populations is continuing.

In some samples, groundmass plagioclase crystals are arranged in a concentric pattern around glomerocrysts. This texture is interpreted to reflect relative movement between the two crystal populations. Because relative movement resulting in the concentric texture could only occur prior to significant crystallization, this feature indicates that; 1) glomerocrysts moved through the gabbroic melt, and 2) plagioclase was a liquidus phase early in the crystallization history of the sill. Local parallel alignment of groundmass plagioclase crystals provides supporting evidence for nucleation and crystallization of plagioclase during emplacement.

Chapter 4: Metamorphism

4.1 Le Fer Formation

The effects of regional metamorphism and contact metamorphism are difficult to distinguish in the host rock sequence. Slaty cleavage is locally developed in shaley units, but foliations are otherwise absent. The most obvious metamorphic effect is the development of a speckled texture in greywacke and siltstone beds in the turbidite sequence adjacent to sill contacts (Figure 5A). The texture reflects the formation of circular areas in which certain phases have been concentrated. In one type, minute granules of magnetite are concentrated in patches generally less than 0.25 mm in diameter. The second type involves the concentration of extremely fine grained chlorite and minor biotite which form fibrous intergrowths reaching 1 mm in diameter. Chlorite-biotite intergrowths are irregular in shape, and may be rimmed by a thin zone of fine grained interlocking quartz grains. The texture is interpreted as a contact metamorphic effect. The development of interlocking quartz grains in quartz-rich lenses and beds reflects recrystallization that may have been driven by either contact or regional metamorphism. The replacement of primary silicate phases in basaltic rocks may in part reflect the effects of autometasomatism during cooling, but the well developed chlorite - actinolite - pumpellyite - sausserite - leucoxene assemblage is indicative of low grade greenschist facies metamorphism. The lack of significant metamorphic effects even in sedimentary rocks immediately adjacent to sill contacts is problematical in light of the fact that the mafic magmas were probably emplaced at temperatures well in excess of 1000 °C.

4.2 Wakuach Gabbro

The degree of alteration of gabbroic rocks is generally low, although certain minerals are particularly prone to replacement. Clinopyroxene may be replaced by actinolite, biotite or chlorite, but is consistently the best preserved phase. Groundmass plagioclase may be partially replaced by clinozoisite or albite, and glomerocrysts often display strong sericitization or sausseritization. Orthopyroxene is usually pseudomorphed by serpentine and chlorite, and magnetite-ilmenite intergrowths may be replaced by leucoxene and hematite. Anorthositic gabbro is particularly prone to alteration, and this is presumably related to the coarse grain size. The secondary assemblage is consistent with low grade greenschist facies metamorphism, but it is possible that much of the alteration represents autometasomatic hydration of the primary silicates.

Chapter 5: Geochemistry

The whole rock major and trace element compositions of 113 gabbro samples from the Howse Lake area were determined to document the compositional variation within and among sills, and to characterize the general geochemical affinities of the rocks. A limited suite of five samples has been used to establish the geochemical characteristics of the host rock basalts in the Howse area. Samples of Willbob and Le Fer volcanic horizons from outside of the study area, and from gabbro sills emplaced in Le Fer turbidites and basalts in the Tait Lake area, were also analyzed for compositional comparisons. Selected rare-earth element (REE) concentrations were determined for samples from the chilled lower margins of the principal sill types, three samples of Willbob basalt, and three samples of host rock basalt. REE data and whole rock analyses are tabulated in Appendix C and D respectively.

5.1 Basalt Geochemistry

In light of the geochronological data discussed earlier, it is apparent that the basaltic rocks of the Howse Lake area are intercalated with turbiditic sediments of the Le Fer Formation. Although the basalts are a volumetrically minor component of the host rock sequence, they are compositionally significant. The geochemical characteristics of Howse basalts are markedly different from other volcanic horizons within the Le Fer Formation, as well as basalts of the Menihek and Willbob Formations. In this section, geochemical comparisons are made with Willbob basalts from the Retty Lake area, and with Le Fer basalts from the Tait Lake area (Figure 2).

The five samples of Howse basalts define an alkalic suite distinct from the tholeiitic nature of the two major periods (eg Le Fer and Menihek) of widespread volcanism represented by basaltic rocks within the Knob Lake Group (cf. Baragar, 1960; Dimroth et al, 1970; Wardle and Bailey, 1981). The basalts are characterized by high total alkalis (Figure 9A), very high Ti and P (Figure 9B), low V (Figure 10A), and light REE enrichment patterns (Figure 10B). The high Ti and P are consistent with the modal abundances of sphene and apatite respectively, and the latter phase is the most probable source of the light REE enrichment trend. The high total iron (Appendix D) in part reflects the abundance of iron oxides. In contrast, the Le Fer and Willbob suites are low in Ti, P and alkalis, and show flat, mid-ocean ridge basalt (MORB)-like REE patterns. Note, however, the negative Eu anomaly of Willbob basalts is absent from the Le Fer patterns.

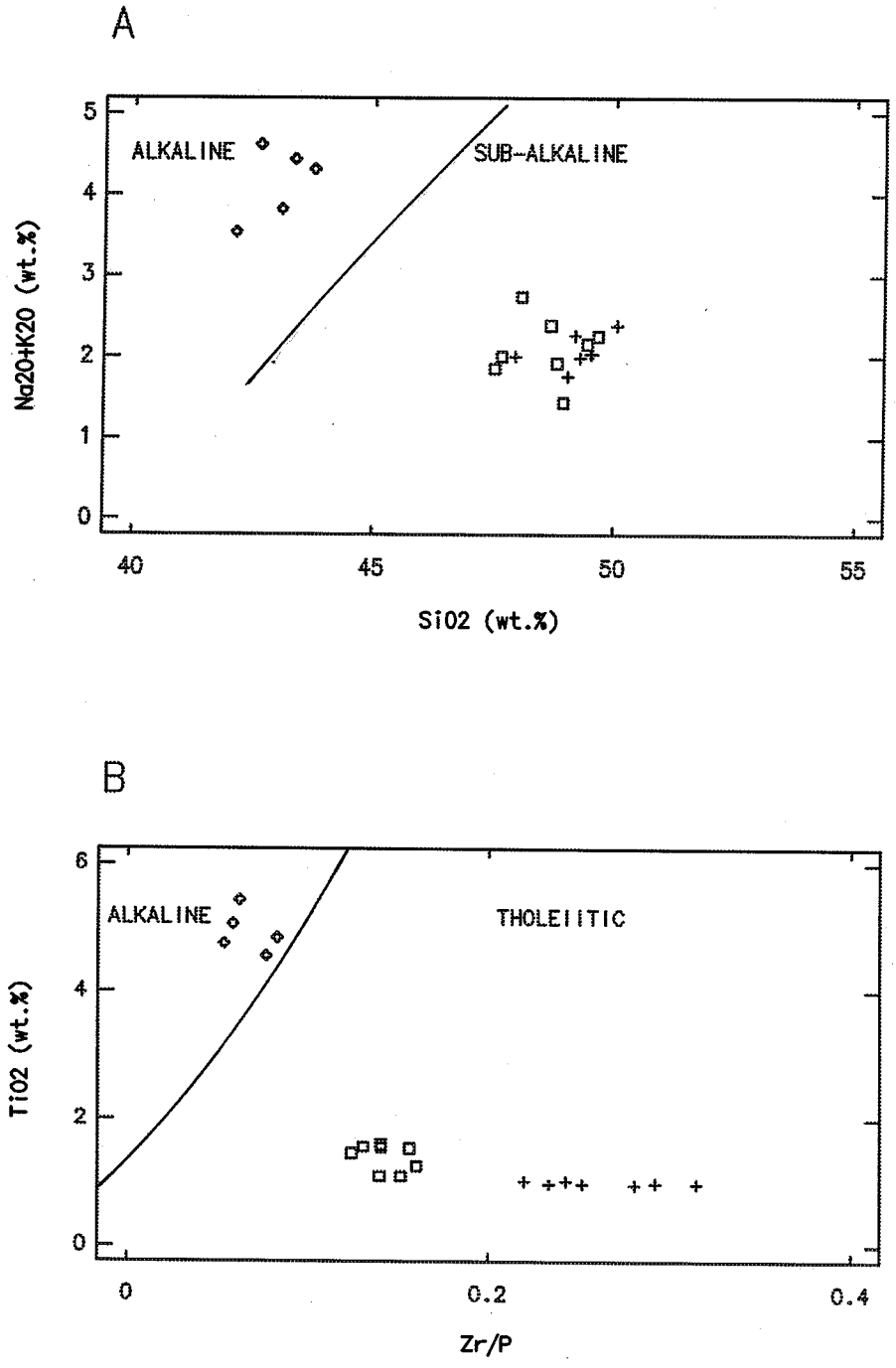

Figure 9. Howse (diamonds), Willbob (boxes), and Le Fer (crosses) basalts plotted in (A) the alkalis-silica diagram of Irvine and Baragar (1971), and (B) the TiO_2-Zr/P diagram of Winchester and Floyd (1976).

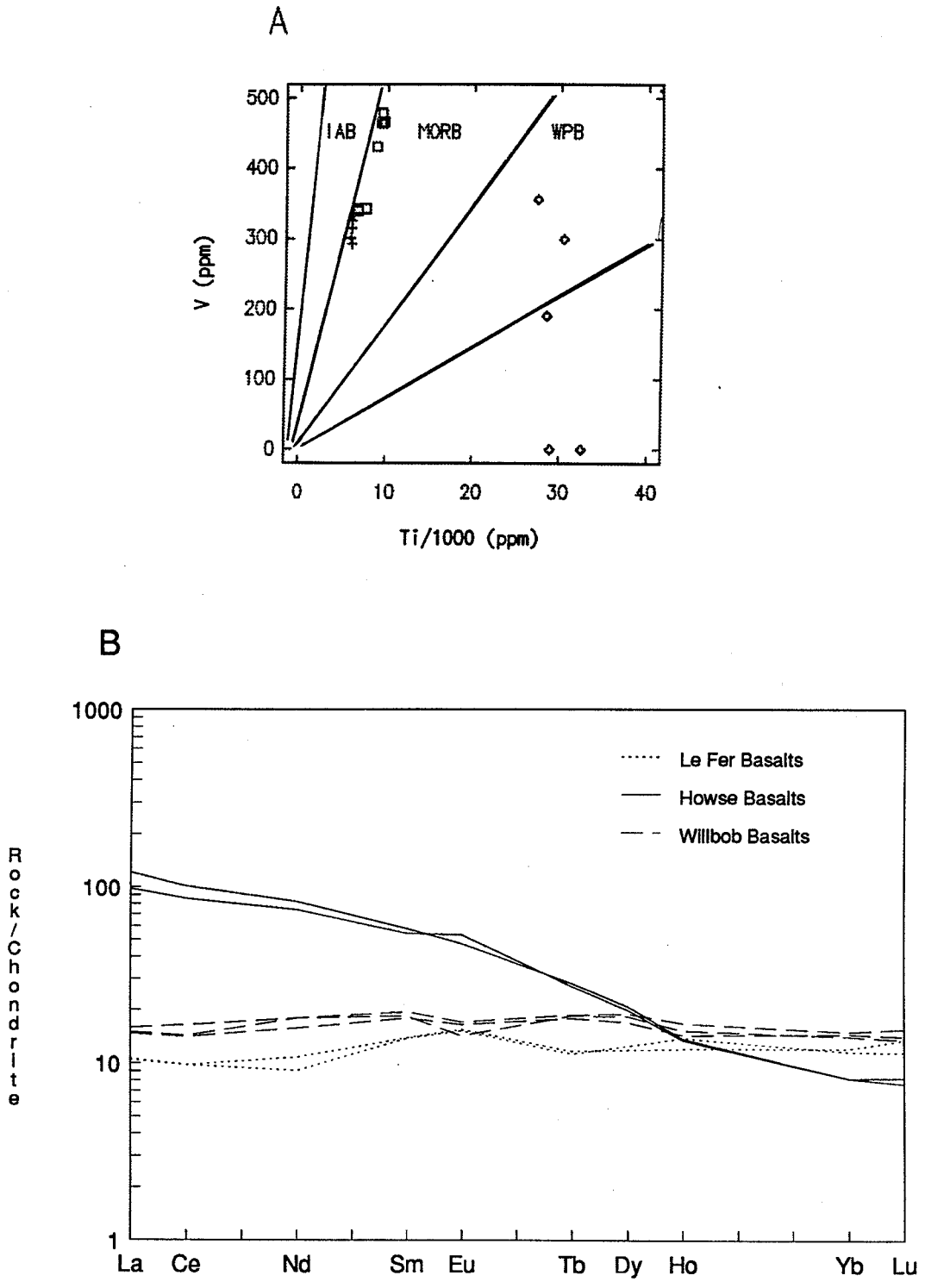

Figure 10. (A) Howse (diamonds), Willbob (boxes) and Le Fer (crosses) basalts plotted in the Ti-V diagram of Shervais (1982). IAB = Island-Arc Basalt; MORB = Mid Ocean Ridge Basalt; WPB = Within Plate Basalt. (B) Rare-earth element patterns of Howse, Willbob and Le Fer basalts (Le Fer samples from Gebert, 1988). Chondrite values from Wakita et al (1971).

In both the alkalis-silica plot of Irving and Baragar (1971) and the TiO_2-Zr/P plot of Winchester and Floyd (1976) the Howse basalts fall within the alkaline fields, whereas the suites of Le Fer and Willbob basalts are tholeiitic. The Howse flows show chemical similarities to within plate basalts (WPB) in the discriminant plots of Shervais (1982) and Pearce and Cann (1973), but the extreme Ti content moves the samples out of the primary WPB fields in the latter (Figure 11). Interestingly, the other suites plot at or near the mid ocean ridge basalt (or ocean floor basalt) - island arc basalt boundary.

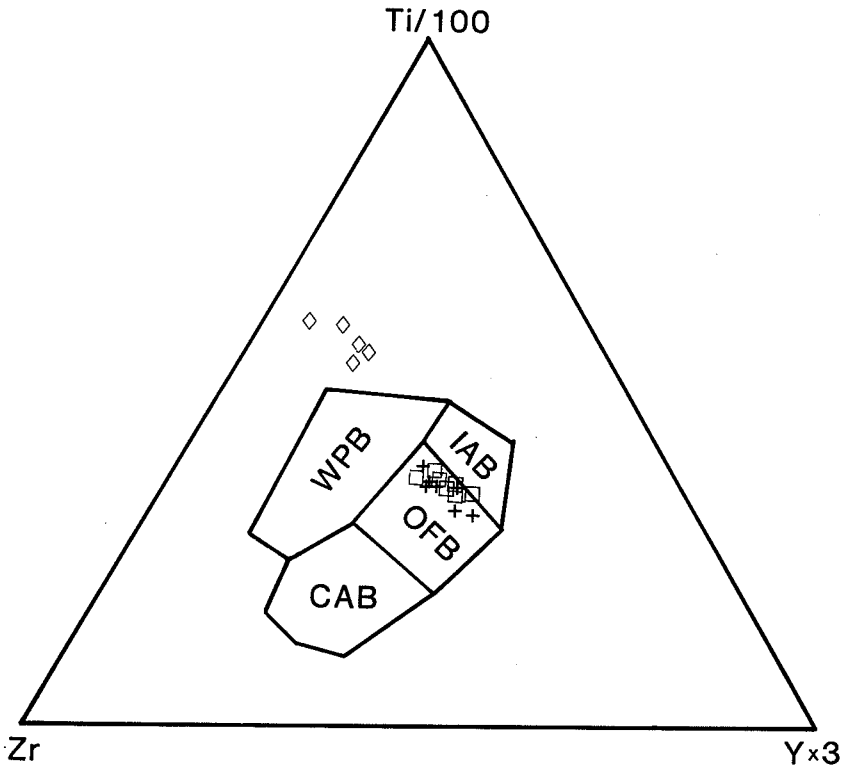

Figure 11. Howse (diamonds), Le Fer (crosses) and Willbob (boxes) basalts plotted in the Ti-Zr-Y discriminant diagram of Pearce and Cann (1973). The high TiO_2 of Howse samples is apparent. WPB = Within-Plate Basalt; IAB = Island-Arc Basalt; OFB = Ocean Floor Basalt; CAB = Calc-Alkaline Basalt

5.2 Gabbro Geochemistry

The main petrological differences among sill lithologies is related to the relative abundance of plagioclase glomerocrysts and phenocrysts. This relationship is also obvious in the whole rock geochemistry of the gabbros. In Figure 12, the decline in MgO and FeO with increasing Al_2O_3 is the result of increasing plagioclase content at the expense of pyroxenes. It can be seen that normal and glomeroporphyritic gabbro have similar ranges except that the latter extends farther toward the values exhibited by anorthositic samples. Similar covariance is exhibited by those elements which occur as major constituents or impurities in pyroxenes or plagioclase, MnO for example (Figure 13).

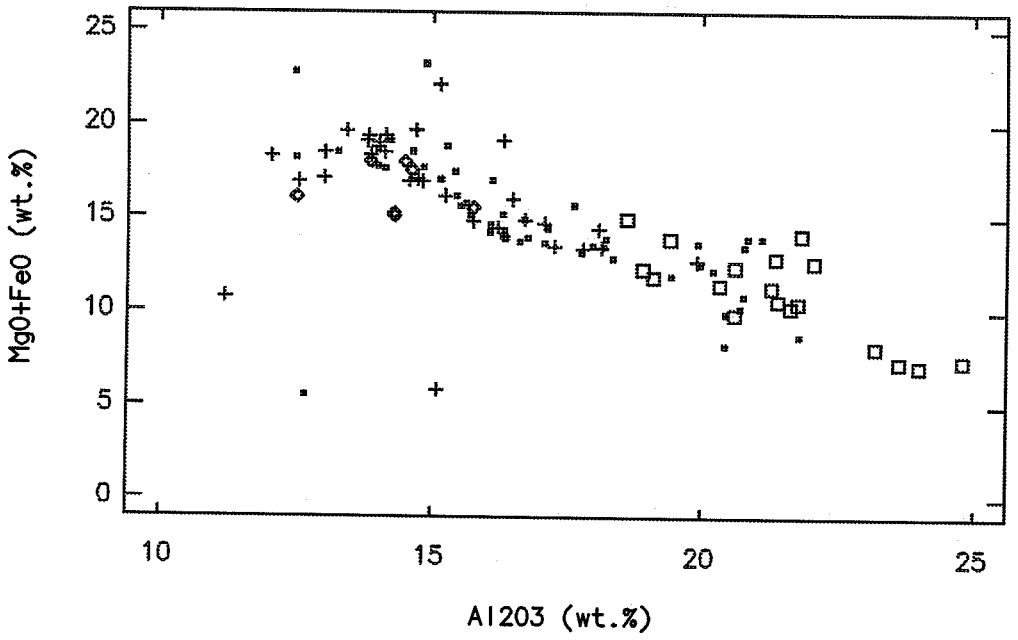

Figure 12. Variation of FeO and MgO with Al_2O_3 in normal (crosses), glomeroporphyritic (points), anorthositic (squares) and Tait Lake (diamonds) gabbros.

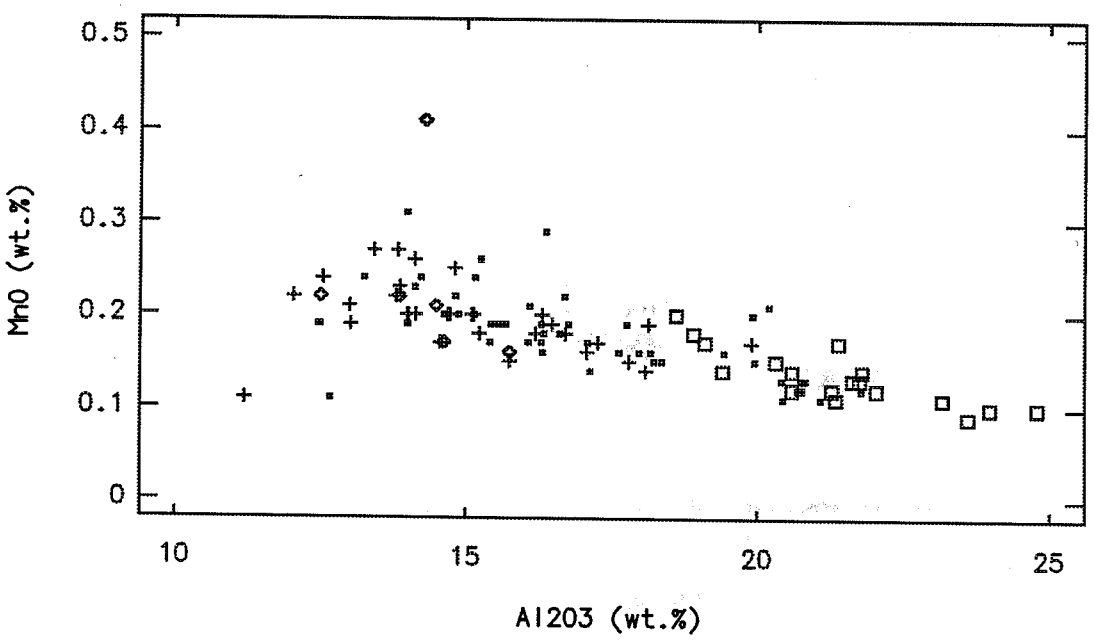

Figure 13. Variation of MnO with Al_2O_3 in normal (crosses), glomeroporphyritic (points), anorthositic (squares) and Tait Lake (diamonds) gabbros.

Conversely, elements which do not substitute into these minerals show only limited variation. The majority of samples of the three main sill types at Howse Lake, along with normal gabbros from the Tait Lake area, show a fairly narrow range of values for SiO_2 and alkalis (Figure 14A), magnesium number (Figure 14B), P_2O_5 and other elements considered indicative of mafic melt evolution. However, the occurrence of minor amounts of more felsic rocks indicates that the melts evolved to a silica-rich liquid. Compositional variation across an example of each of the three main sill types is illustrated in Figure 15. Samples represent glomerocryst-free matrices in the case of the glomeroporphyritic and normal gabbro sills, and matrix + glomerocrysts in the anorthositic sill. Again it is clear that plagioclase and augite are controlling much of the variability of the rocks. Since normal and glomeroporphyritic samples are glomerocryst free, the covariations illustrated must reflect variable plagioclase-augite ratios in the matrix of samples. The wide range of Al_2O_3 values and petrographic evidence of early matrix plagioclase crystallization suggests

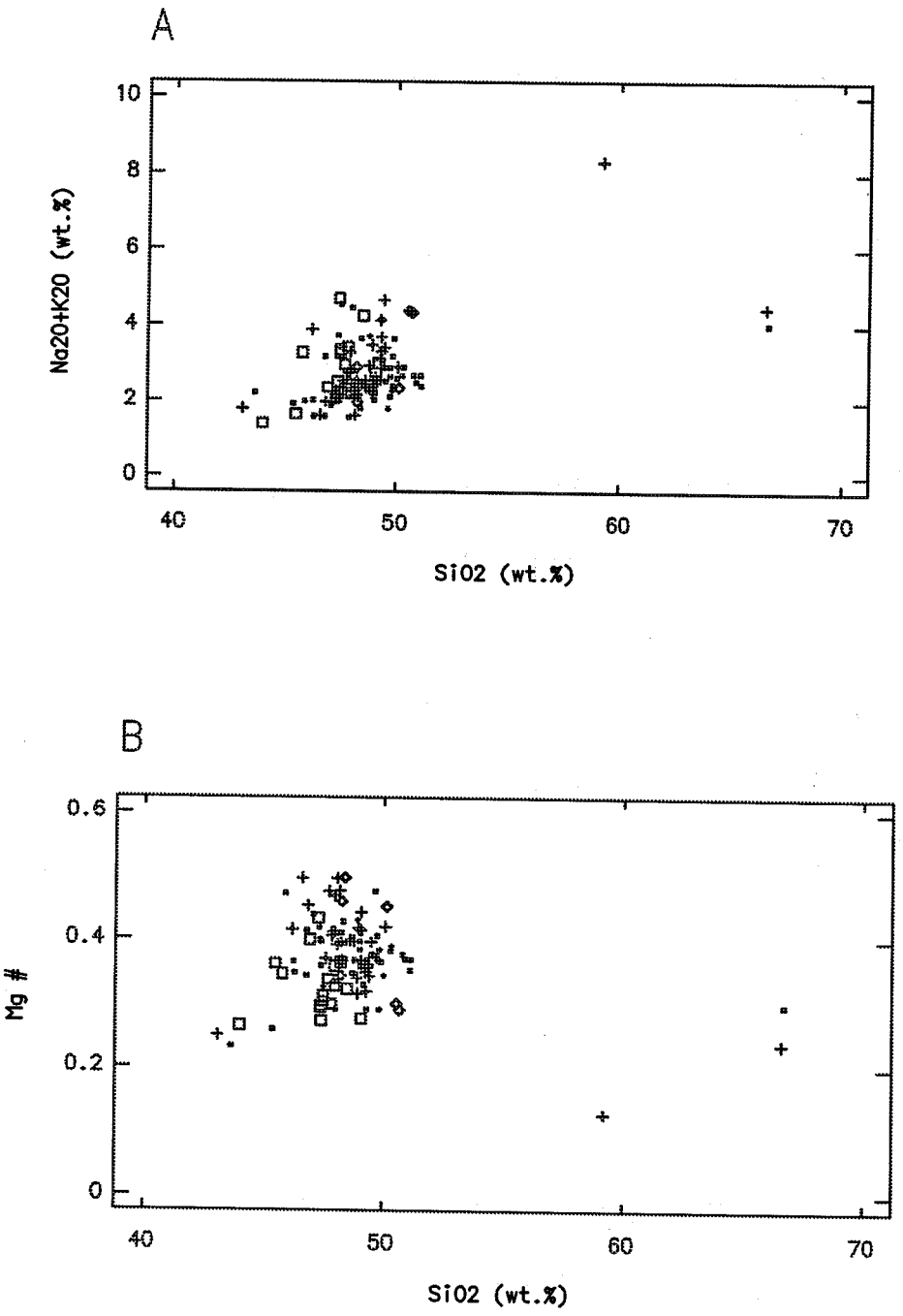

Figure 14. Plots of silica-alkalis (A) and silica-Mg # (B) showing generally limited compositional variation of normal (crosses), glomeroporphyritic (points), anorthositic (squares) and Tait Lake (diamonds) gabbros.

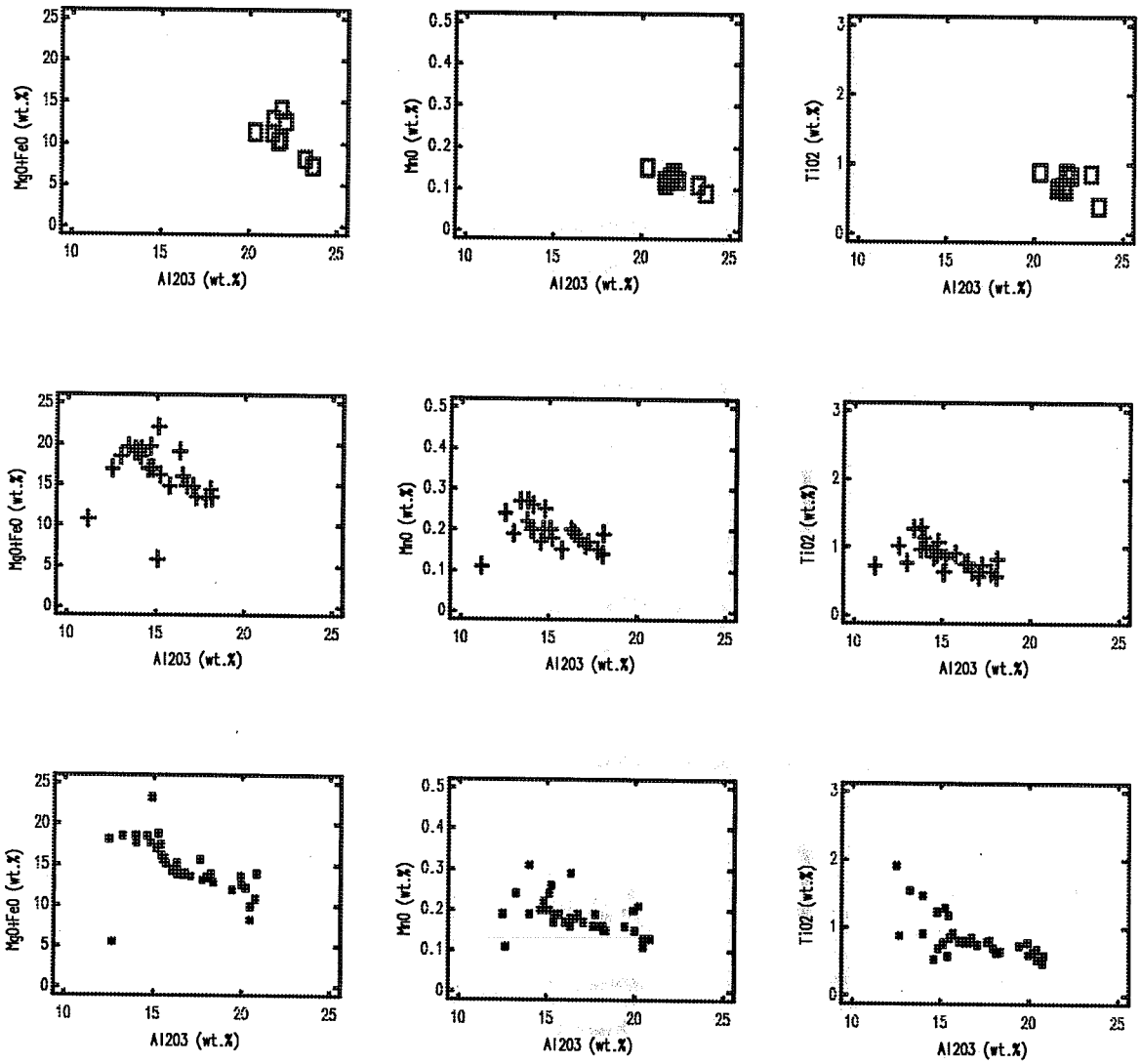

Figure 15. Variation in MgO+FeO, MnO and TiO_2 with Al_2O_3 in each of the main sill types; anorthositic gabbro (boxes), glomeroporphyritic gabbro (points) and normal gabbro (crosses).

that much of the compositional variation exhibited by the gabbros can be attributed to variable accumulation of matrix plagioclase.

Comparison of the silica-alkalis plots for basalts (Figure 9A) and gabbros (Figure 14A) illustrates the general geochemical similarity of Le Fer basalt, Willbob basalt, normal gabbro and glomeroporphyritic gabbro. REE patterns for samples of the chilled margins of each type of sill are plotted in Figure 16. The REE patterns of gabbro samples are very similar to the flat patterns shown by Willbob basalts,

although the anorthositic gabbro is without the negative Eu anomaly shown by the other rocks. The Eu anomaly points to a history of plagioclase fractionation prior to or during ascent of the magmas which formed the Willbob basalts and normal and glomeroporphyritic gabbro. The lack of a Eu anomaly in anorthositic gabbro is problematic in view of the fact that the sample represented chilled gabbro showing less than 1% glomerocrysts. It is possible that resorption of a portion of the glomerocrysts carried by the melts during ascent and emplacement erased the anomaly. Such a process might also explain the relative sizes of anomalies exhibited by normal and glomeroporphyritic samples. Field evidence suggests that normal gabbros were emplaced prior to glomeroporphyritic gabbros, and presumably the barren melts reflect extraction during the early stages of plagioclase fractionation in the feeder chamber. Hence the Eu depletion should be greater in glomeroporphyritic melts.

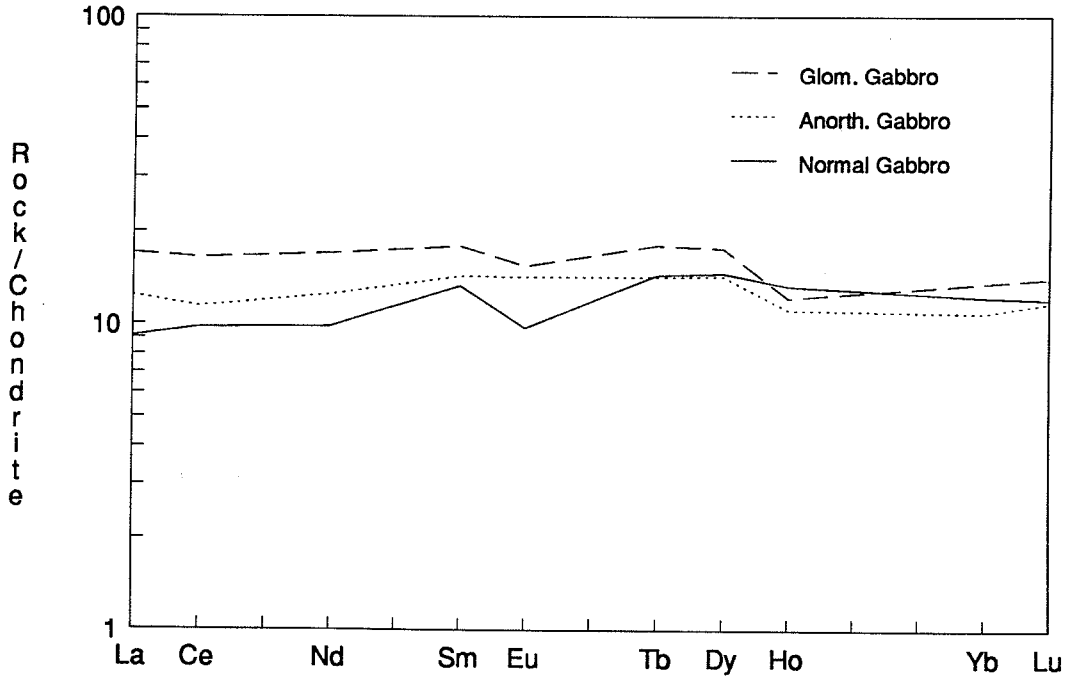

Figure 16. REE patterns of samples of the chilled lower margins of each of the main sill types. Chondrite values from Wakita et al (1971).

Chapter 6: Petrogenesis

Several interpretations regarding the tectonic setting of the Labrador Trough have been advanced. Baragar and Scoates (1981) suggested that the package was developed in an ensialic rift localized near the outer eatern margin of the Superior Craton. These authors envisage development of a proto-oceanic basin that failed to open completely. Wardle and Bailey (1981) and others suggest the sequence developed through rifting of the passive margin of the Superior Craton and development of an oceanic basin. In this model, the Knob Lake Group represents miogeosynclinal sedimentation along the margin of the Superior craton, and the Doublet basalts and Wakuach Gabbro are considered the products of oceanic rift magmatism. More recently, a foredeep model has been proposed in which the upper members of the Knob Lake were deposited on the flanks of a foredeep basin and the Doublet Group represents axial zone volcanism (Hoffman, 1987). Gabbroic sills of the Montagnais Group intrude both axial zone and flank sediments, and represent intrusive equivalents of the axial volcanism. Neither model satisfactorily explains the tectonic setting or significance of the amphibolite grade Laporte Group, although some authors have suggested that this sequence is the temporal eugeosynclinal equivalent of the Knob Lake Group, and the Doublet Group developed above both Laporte and Knob Lake Groups (Dimroth et al, 1970; Wardle and Bailey, 1981).

6.1 Le Fer Basalts

Previous mapping has assigned the host rock sequence described above to the Menihek Formation, a volcanic-sedimentary succession which forms the uppermost unit of the Knob Lake Group. However, Menihek basalts have been described as tholeiitic in character (Baragar, 1967; Dimroth, 1978; Wardle and Bailey, 1981), whereas initial analytical work indicates that Howse Lake volcanics are alkaline in nature. As discussed earlier, age relationships indicate that the Menihek Formation is younger than the Howse Lake intrusions. Consequently, the host rock succession is assigned to the Le Fer Formation, a sequence which is considerably older than the Menihek Formation. This implies the existence of an unrecognized northwesterly-trending thrust fault at the western limit of glomeroporphyritic sills near Attikamagen Lake (Figure 4).

The tholeiitic nature of Le Fer basalt in the Tait Lake area of the Ferrum Zone confirms the results of numerous previous studies of the chemical affinities of basaltic volcanism in the central Labrador Trough. It is apparent that the alkali basalts of Howse Lake are geochemically anomalous in terms of the predominant type of volcanic activity. One explanation is that the Howse Zone represents a lower stratigraphic level of the Le Fer Formation than is exposed in the Ferrum Zone. The absence of Ferriman Subgroup strata in the Howse Zone offers support for this interpretation. Howse

basalts might then represent the earliest products of rift-related volcanism which evolved into the more prevalent oceanic tholeiites with continued rifting.

6.2 Wakuach Gabbro

Textural and compositional differences between the two populations of plagioclase crystals in glomeroporphyritic gabbro reflect different crystallization environments. Glomerocrysts bear a striking resemblance to anorthositic cumulates (cf Wager et al, 1960; Morse, 1969), and it is probable that they represent the products of fractional crystallization and accumulation of plagioclase in a feeder chamber at depth. Melt expelled from the chamber entrained plagioclase crystals and aggregates which were hydraulically concentrated towards the centre of flow during ascent and emplacement (Baragar, 1960; Komar, 1972). The central accumulation of aggregates resulted in the general pattern of non-porphyritic to sparsely-porphyritic marginal zones, and increasing numbers of glomerocrysts toward the center of the sills. The magmatic pulse may have continued to crystallize plagioclase during emplacement, and movement of glomerocrysts toward the central part of the flow through melt containing plagioclase crystals and nuclei produced the concentric arrangement of groundmass crystals observed. Sharp internal contacts indicate that coarse grained anorthositic gabbro forming the central portions of many glomeroporphyritic sills has developed through emplacement of a second magmatic pulse which cooled slowly as a result of the insulating effect of the earlier intrusion. The coarse grained nature of anorthositic gabbro forming discrete sills may have similarly developed through slow cooling, since these lithologies appear to represent the youngest magmatic incursion and previous injections might have heated the host rock package.

The mineralogical and chemical similarities of normal and glomeroporphyritic gabbro, and their close spatial association, suggests that they are comagmatic. Normal gabbro enclaves within anorthositic gabbro indicate that the former, at least locally, predates the latter. It is probable that crystal-free liquids were removed prior to, or during the first stages of plagioclase fractionation in the feeder chamber. The development of localized phase layering is thought to reflect limited *in situ* fractional crystallization, and this process has contributed to the evolution of siliceous differentiates within the sills. Plagioclase appears to have been the earliest phase to crystallize, and variable accumulation of this phase has led to much of the compositional variation exhibited by the sills. Assimilation of Le Fer sediments may have been an additional factor in the differentiation process, and is perhaps responsible for the

accumulation of this phase has led to much of the compositional variation exhibited by the sills. Assimilation of Le Fer sediments may have been an additional factor in the differentiation process, and is perhaps responsible for the commonly elevated sulphide content of many of the gabbroic rocks.

Textural and chemical similarities between Wakuach gabbros and Willbob basalts offer strong evidence for consanguinity. The lack of anorthositic gabbro sills in the Doublet Terrane may be related to the stratigraphic level represented by the present erosional surface. It is possible that the level of sill emplacement in the stratigraphic sequence was influenced by crystal load, with heavily charged magmas restricted to lower stratigraphic levels due to viscosity constraints. This might explain the localization of anorthositic gabbro in contrast to the broad range of normal gabbro (and metagabbro in the Doublet Terrane), if the Howse Zone represents a deeper stratigraphic level than either the Ferrum Zone or Doublet Terrane.

Chapter 7: Economic Geology

Base metal exploration of the Labrador Trough has been conducted more or less continuously for almost fifty years, and although several significant prospects have been discovered, along with virtually hundreds of showings, none have proven economic. In the past four years the recognition of suitable environments for precious metal mineralization has led to a resurgence of exploration activity in the Labrador Trough. The announcement by industry of anomalous Platinum Group Element (PGE) concentrations in sulphide enriched zones hosted by glomeroporphyritic gabbro sills in the northern Labrador Trough (Avison et al, 1986; results also reported in Clark, 1987), has sparked considerable interest in this distinctive lithology. The evaluation of the economic potential of the Howse Lake area was concerned primarily with an investigation of the precious metal potential of the Wakuach sills and, in particular, the sulphide enriched zones they host.

7.1 Sulphide Occurrences

Pyrite and pyrrhotite are constituents of most metasedimentary rocks of the area. In siltstone and quartzite layers these phases, along with minor chalcopyrite, occur as fine grained disseminations, generally occupying less than 5 volume % of samples. In shale horizons, sulphides appear to be less abundant overall, but local concentrations occur as 5-10 mm thick lenses, discontinuous laminae, or layers of semi-massive to massive pyrite and pyrrhotite. Similar massive sulphide laminae and layers, albeit on a larger scale, have been described as sulphide facies iron formation in the adjacent Frederickson Lake area, Québec, and assigned to the upper Menihek Formation (Gebert, 1988). No such extensive or continuous sediment-hosted massive sulphide units were observed at Howse Lake. Sulphide occurrences in other host rock units are very minor; pyrite forms 1 to 10 mm - sized circular, apparently epigenetic, blebs in volcanic horizons, but was not observed in pyroclastic units.

Sulphide minerals are ubiquitous accessory phases in all gabbroic lithologies at Howse Lake. Pyrrhotite predominates, but may be accompanied by minor chalcopyrite and pentlandite in sulphide enriched zones. Typically, pyrrhotite occupies 1-2 volume % of samples as fine, disseminated grains interstitial to, or enclosed by, silicate minerals. Larger interstitial pyrrhotite grains, particularly in coarse grained anorthositic lithologies, may show exsolution blebs or partial rinds of chalcopyrite.

Local sulphide concentrations were observed in most lithologies, but appear to be best developed in normal and sparsely glomeroporphyritic gabbro. Sulphide phases may constitute up to 25% of the rock in irregular zones or lenses, and less commonly, in stratiform horizons which range in thickness from 20 centimeters to 1 meter. The continuity of the horizons is unknown; most can be traced along strike across individual outcrops, but the poorly exposed nature of the area prevented correlation between outcrops. Net-textured pyrrhotite predominates, and may be intergrown with small grains of chalcopyrite or, less commonly, pentlandite. The latter minerals also occur as exsolution blebs or flames within pyrrhotite. Stratiform sulphide enriched horizons are best developed in marginal glomeroporphyritic gabbro, and are commonly associated with phase layering defined by alternating plagioclase- and pyroxene-rich layers. Minor sulphide enrichment, erratically developed at internal intrusive contacts between glomeroporphyritic gabbro and the anorthositic gabbro of a subsequent injection, was observed at several locations.

Sulphides are also present in quartz-chlorite veins locally developed within the sills. Pyrite is a common accessory phase in the veins and is locally joined by galena and chalcopyrite, but the total amount of sulphide is low. Both galena and pyrite occur as coarse, subhedral to anhedral grains, while chalcopyrite forms finer disseminations. The mineralogy of the veins, and their sharp and generally discordant nature, contrasts with the more diffuse veins and bands described earlier, and suggests a fracture-filling origin. Galena from a discordant quartz-chlorite vein in the same anorthositic gabbro horizon that provided the U-Pb zircon age, yielded a model Pb-Pb age of 1743-1784 Ma (Clarke and Thorpe, 1987) which is consistent with an epigenetic origin.

7.2 Sulphur Isotopes

Pyrite-pyrrhotite lenses and layers in the host rock sequence are concordant to bedding and are deformed in the same manner as enclosing shale. This suggests a synsedimentary origin. Gebert (1988) similarly considered Menihek sulphides in the Frederickson Lake area to be synsedimentary. No samples of this type of occurrence from Howse Lake were subject to sulphur isotope analysis. However, reported isotopic compositions in pyrrhotite from sulphide facies iron formation in the Frederickson Lake area have an average $\delta^{34}S$ value of +3.5 per mil (Gebert, 1988) and a similar average value of +3.7 per mil was reported by Cameron (1983).

The fine grained, anhedral nature of disseminated pyrite and pyrrhotite grains in siltstone and quartzite layers also suggests a synsedimentary origin. Sulphide separates from samples of greywacke produced $\delta^{34}S$ values ranging from +10.7

to +22.9 (Figure 17), with an average value of +16.0. The large degree of scatter in $\delta^{34}S$ values may in part reflect recrystallization fractionation during regional or contact metamorphism, although the differences would seem too great to be due entirely to this process (cf Kajiwara et al). Despite the scatter of data, disseminated sulphides in the host metasedimentary rocks appear to be substantially enriched in ^{34}S relative to sulphide facies iron formation in the Frederickson Lake area. It is possible that the difference in isotopic compositions reflect variable contributions of precipitated and detrital sulphide minerals to the total sulphide contents of the rocks.

Sulphides in gabbroic lithologies show magmatic textures and it is apparent that they represent separation of immiscible sulphide liquid from the silicate magma. In the case of the minor amounts of disseminated sulphide found in all units, immiscibility occurred largely during late stage crystallization of interstitial liquid. In contrast, larger concentrations of sulphides probably reflect segregation of sulphide droplets during crystallization of the silicate framework. The sulphur content of the initial magma is unknown, but sulphur isotope data indicate that sedimentary sulphur was incorporated into the sills. Consequently, segregation of sulphide liquid may reflect saturation resulting from assimilation of host rock sulphur.

Gebert (1988) found little difference between the isotopic composition of glomeroporphyritic gabbro-hosted, massive Cu-Ni sulphide occurrences and the host sulphide facies iron formation of the Frederickson Lake area. However, a whole rock sulphur analysis of 'ordinary' gabbro returned a $\delta^{34}S$ value of +2.2 per mil, and Gebert concluded that some contribution of sedimentary sulphur to the Cu-Ni sulphides was probable, possibly through volatilization of sulphur during metamorphism of enclosing metasediments or metasedimentary xenoliths. Isotopic compositions of chalcopyrite-pyrrhotite pairs from sulphide enriched samples of the three main sill types at Howse Lake are illustrated in Figure 17, along with values for host rock samples. All samples show elevated $\delta^{34}S$ values relative to the magmatic range of -1 to +2 per mil (Ohmoto and Rye, 1979) and it is clear that sulphide enriched zones in all gabbro types have benefited from the addition of sedimentary sulphur. The number of analyses and the wide scatter of values precludes conclusions regarding differences in the isotopic composition of sulphides hosted by the various sill types. However, it is interesting to note the apparent trend of increasing $\delta^{34}S$ values from anorthositic gabbro to normal gabbro. The average ^{34}S composition of metasedimentary sulphides is sufficient

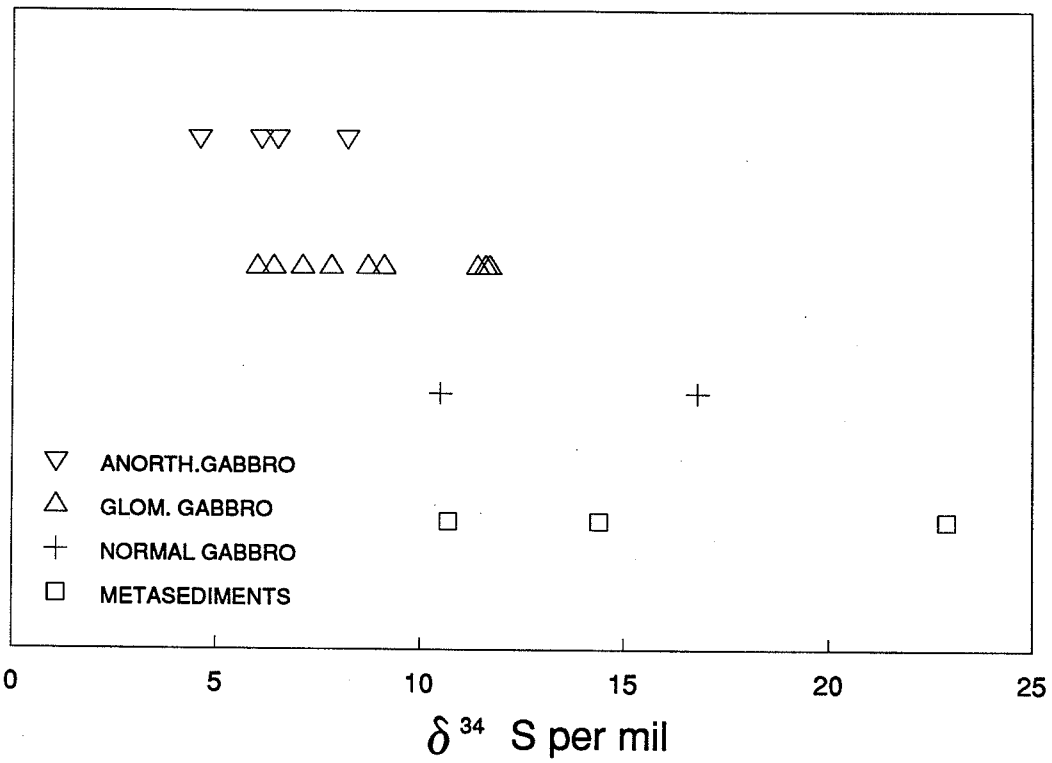

Figure 17. Isotopic composition of sulphide minerals in sills and host rocks of the Howse Lake area.

to produce even the rather high values shown by sulphide enriched normal gabbro through assimilation of host rock sulphur. If the elevated values are the result of sulphur assimilation, then the variation of ^{34}S in different lithologies may be qualitatively, albeit simplistically, explained by the variable contribution of extraneous sulphur. The degree of assimilation is linked to the temperature and crystallization history of the intruded magma, and it might be expected that thick sills which crystallized over a long time period will have the greatest potential for incorporating large amounts of sedimentary sulphur. Normal gabbro sills carried the smallest crystal load, the heat of crystallization of constituent minerals would have a greater effect on the rate of cooling than in an anorthositic gabbro sill which was emplaced carrying 30-50% plagioclase crystals. The crystal load of glomeroporphyritic gabbro is intermediate between anorthositic and normal gabbro, and hence the amount of sedimentary sulphur assimilated is also intermediate.

7.3 Platinum-Group Element Potential

The PGE potential of the area was assessed through determination of the Pt, Pd and Au content of selected samples of all major lithologies. Sample locations are shown on the accompanying map, and assay results and brief sample descriptions are tabulated in Appendices A and B. Samples are grouped according to lithological type. Cu, Ni and Pt+Pd profiles for sample sections across normal and glomeroporphyritic gabbro sills exposed at the southern end of Howse Lake are illustrated in Figure 18. In Figure 18A, Cu, Ni and Pt+Pd peaks at 218m corresponds to a 20 cm thick stratiform horizon in sparsely glomeroporphyritic gabbro containing 15 volume % sulphides. Unlike most samples which show anomalous values, the Pt+Pd peak at 305m represents sparsely glomeroporphyritic gabbro with 1 volume % sulphides. The normal gabbro section of Figure 18B shows little variation in Cu, Ni or Pt+Pd, although slightly elevated Pt+Pd values occur near the top of the sill. Samples taken during reconnaissance traversing generally show low concentrations of the precious metals and the few anomalous values are associated with sulphide enriched zones. Average metal values are illustrated in Figure 19, and there is an apparent trend of decreasing chalcophile metal concentration from anorthositic gabbro, through glomeroporphyritic and normal gabbro, to metasedimentary rocks. If the $\delta^{34}S$ values for the three main sill types reflect variable sulphur assimilation, then the trend in metal concentrations may represent increasing sulphide-magma ratios from anorthositic gabbro to normal gabbro.

The primary mechanism of PGE concentration in magmatic deposits is generally considered to be sulphide immiscibility, since the PGE will be strongly partitioned into a sulphide liquid relative to silicate magma. Sulphide enriched samples at Howse Lake generally show the highest metal values and it is apparent that immiscible sulphide liquid scavenged minor amounts of PGE from the silicate melt. However, metal values, even in sulphide enriched zones, are relatively low and there appears to be little potential for economic mineralization in these sills. The low Cu-Ni-PGE contents may result from dilution of metal concentrations through assimilation of large amounts of sedimentary sulphur. High sulphide to silicate liquid ratios are supported by the sulphur isotope data discussed previously. $\delta^{34}S$ values from Howse Lake sills, particularly normal and glomeroporphyritic lithologies, indicate that the isotopic composition of sulphides was largely controlled by the composition of sedimentary sulphur. It is also possible that immiscible sulphide liquid simply did not equilibrate with sufficient quantities of silicate magma to produce a large concentration in the PGE.

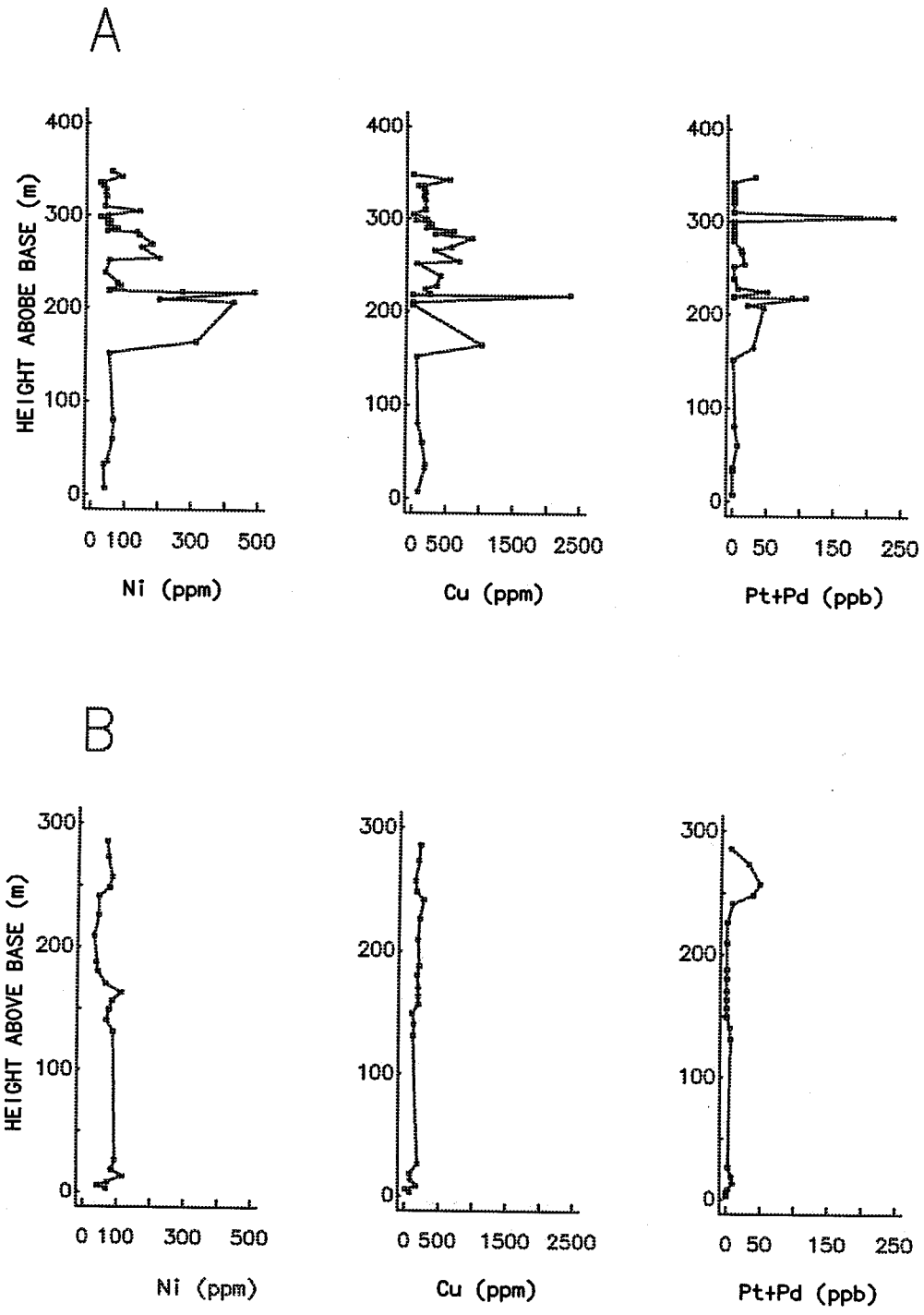

Figure 18. Metal concentration profiles across well exposed glomeroporphyritic (A) and normal (B) gabbro sills. (A) represents sample series F14 and F16, (B) represents sample series F876 and SH1. See map for series locations.

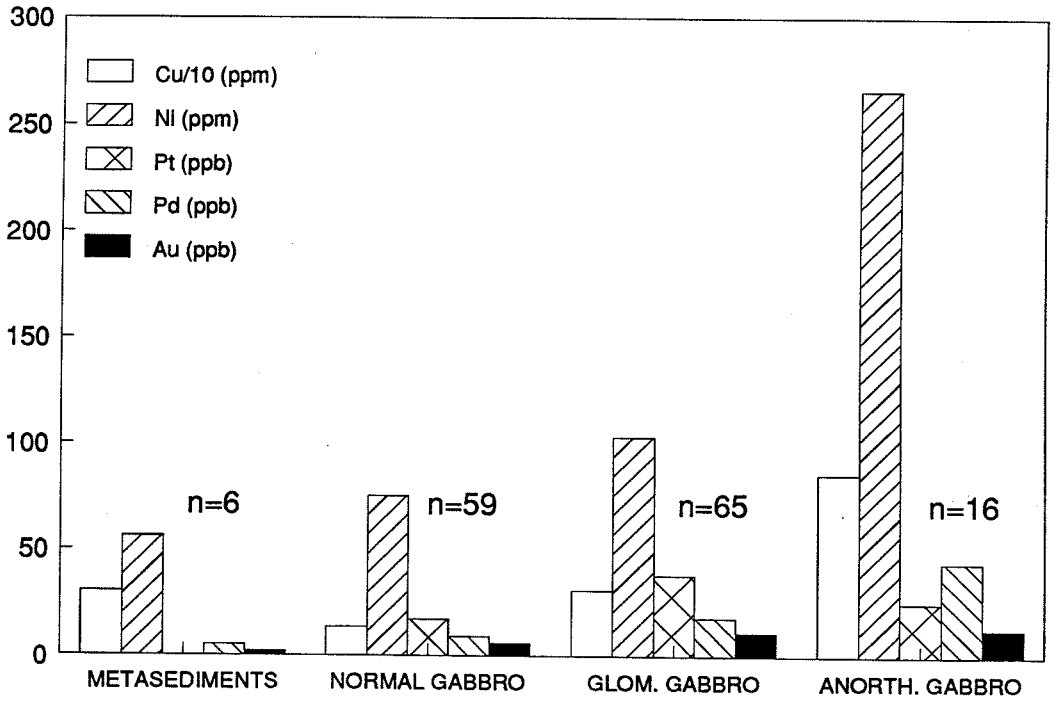

Figure 19. Average metal values for the three principal gabbro lithologies and country rocks. n = number of samples.

References

Avison, T., Ferderber, P. and Scott, F. (1986) Platinum group and gold discoveries in the Labrador Trough. Paper presented at the Séminaire d'information of the Direction générale de l'Exploration géologique et minérale, Ministère de l'Energie et des Ressources, Québec.

Baragar, W.R.A. (1958) Ahr Lake map-area, Québec. Geological Survey of Canada, Paper 57-7.

_____ (1960) Petrology of basaltic rocks in part of the Labrador Trough. Geological Society of America, Bulletin 71, p. 1589-1643.

_____ (1967) Wakuach Lake map area, Québec-Labrador. Geological Survey of Canada, Memoir 344.

_____ and Scoates, R.F.J. (1980) The Circum-Superior belt: a Proterozoic plate margin. In Precambrian Plate Tectonics. Edited by A. Kroner. Elsevier, Amsterdam, p. 297-329.

Cameron, E.M. (1983) Genesis of Proterozoic iron formation: sulphur isotope evidence. Geochim. Cosmochim. Acta, 47, p. 1069-1074.

Clarke, T. (1987) Platinum Group Element occurrences of the Labrador Trough. Ministère des Richesse Naturelles du Québec, Document de promotion, 18.

_____ (1984) Géologie de la région du lac Cambrien, territoire du Nouveau Québec. Ministère de l'Energie et des Ressources, ET 83-02.

_____ and Thorpe, R. (1987) Lead isotope galena ages from the Labrador Trough (abst.). Geol. Assoc. Can. - Mineral. Assoc. Can. Program with Abstracts, v. 12, p. 33.

Dimroth E. (1970) Evolution of the Labrador geosyncline. Geological Society of America, Bulletin 81, p. 2717-2742.

_____ (1978) Labrador Trough Area. Ministère des Richesse Naturelles, Québec, Rapport Géologique 193.

_____, Baragar, W.R.A., Bergeron, R. and Jackson G.D. (1970) The filling of the Labrador Geosyncline in A.J. Baer (ed.) Symposium on basins and geosynclines

of the Canadian Shield. Geological Survey of Canada, Paper 70-40, p. 45-142.

Evans, J.L. (1978) An alkalic volcanic suite of the Labrador Trough, Labrador. Unpublished M.Sc. thesis, Memorial University of Newfoundland, St.John's, Newfoundland.

Findlay, J.M., Watanabe, D. H. and Birkett, T.C. (in prep.) Ages of the Wakuach Gabbro and Nimish Formation, Western Labrador.

Frarey M.J. (1967) Willbob Lake and Thompson Lake map-area, Québec. Geological Survey of Canada, Memoir 348.

_____ and Duffell S. (1964) Revised stratigraphic nomenclature for the central part of the Labrador Trough. Geological Survey of Canada, Paper 64-25.

Fryer, B.J. (1972) Age determination in the Circum-Ungava geosyncline and the evolution of Precambrian banded iron formations. Can. J. Earth Sci., 9, 652-663.

Gebert, J. (1988) The metallogeny of Cu-Ni and Zn-Cu-Pb deposits of the Frederickson Lake area, central Labrador Trough. Unpublished M.Sc. thesis, McGill University, Montreal, Québec.

Hoffman, P.F. (1987) Proterozoic foredeeps, foredeep magmatism and giant iron formation. in A. Kroner (ed.) Proterozoic Lithospheric Evolution, Amer. Geophys. Union Geodynamic Series, 17, p. 85-98.

Irvine T.N. and Baragar W.R.A. (1971) A guide to the chemical classification of the common volcanic rocks. Canadian Journal of Earth Sciences, 8, p. 523-548.

Kajiwara, Y., Sasaki, A. and Matsubaya, O. (1981) Kinetic sulphur isotope effects in the thermal decomposition of pyrite. Geochem. Journal, 15, p. 193-197.

Komar, P.D., (1972) Flow differentiation in igneous dikes and sills: Profiles of velocity and phenocryst concentration, Geological Society of America, Bulletin, 83, p. 3443-3448.

Morse S.A. (1969) The Kiglapait layered intrusion, Labrador. Geological Society of America, Memoir 112.

Ohmoto, H. and Rye, R.O. (1979) Isotopes of sulphur and carbon in H.L. Barnes (ed.) Geochemistry of hydrothermal ore deposits. John Wiley and Sons: Toronto, p. 509-567.

Pearce, J.A. and Caan, J.R. (1973) Tectonic setting of basic volcanic rocks determined using trace element analyses. Earth and Planetary Science Letters, 19, p. 290-300.

Percival, J.A. and Girard, R. (1988) Structural character and history of the Ashuanipi Complex in the Schefferville area, Québec-Labrador in Current Research, Part C. Geological Survey of Canada, Paper 88-1C, p. 51-60.

Shervais, J. W. (1982) Ti-V plots and the petrogenesis of modern and ophiolitic lavas. Earth and Planetary Science Letters, 59, p. 101-118.

Wager L.R., Brown G.M. and Wadsworth W.J. (1960) Types of igneous cumulates. Journal of Petrology, 1, p. 73-85.

Wakita, H., Rey, P. and Schmitt, R.A. (1971) Abundances of 14 rare-earth elements and 12 other trace elements in Apollo 12 samples: five igneous and one breccia rocks and four soils. Proc. 2nd Lunar Sci. Conf., p.1319-1329.

Wardle R.J. (1982) Geology of the South-Central Labrador Trough. Newfoundland Department of Mines and Energy, Mineral Development Division, Map 82-6.

_____ and Bailey D.G. (1981) Early Proterozoic sequences in Labrador. in F.H.A. Campbell (ed.) Proterozoic Basins Canada. Geological Survey of Canada, Paper 81-10, p. 331-359.

_____, Ryan, B., Nunn, G.A.G. and Mengel, F.C. Labrador segment of the Trans-Hudson Orogen: crustal development through oblique convergence and collision in The Trans-Hudson Orogen of North America: Lithotectonic correlations and evolution. Geol. Assoc. Can., Special Paper (in press).

Winchester J.A. and Floyd P.A. (1976) Geochemical magma type discrimination: application to altered and metamorphosed basic igneous rocks. Earth and Planetary Science Letters, 28, p. 459-469.

Appendix A: Assay Results

The majority of samples listed below were analyzed by Bondar-Clegg & Company Ltd. using the following techniques:

Element	Method	Detection Limit
Co	atomic absorption	1 ppm
Ni	atomic absorption	2 ppm
Cu	atomic absorption	1 ppm
Cr	X-ray Fluorescence	2 ppm
Pt	Fire Assay, DCP	15 ppb
Pd	Fire Assay, DCP	2 ppb
Au	Fire Assay, DCP	1 ppb

Samples denoted by an asterisk were analyzed by fire assay-neutron activation analysis by X Ray Assay Laboratories Ltd. with the following detection limits:

Pt: 5 ppb
Pd: 5 ppb
Au: 1 ppb

Sample	Cu	Ni	Co	Cr	Pt	Pd	Au
Howse Basalts							
F18-25	54	<2	80	<2	<15	<5	<2
F20-9*					14	<5	2
Anorthositic Gabbro							
B32-7*	330	190	46	350	<5	8	<2
F13-3A	810	148	29	22	16	40	12
F871-2	1030	311	43	33	<15	30	15
F871-3	67	52	16	103	<15	<2	<1
F871-4	88	66	24	34	<15	3	2
F871-5	153	64	23	48	<15	7	<1
F872-1	45	13	31	<2	<15	<2	<1
H2-3*	130	83	45	50		4	<2
H2-6*	2500	640	66	100	20	32	14
H3-5*	4000	1500	120	60	50	250	61
W24-4	3465	442	41	42	28	106	34
W25-7B	266	63	31	51	<15	<2	1
B23-15A	14	32	18	58	<15	<2	2
F20-7B	176	39	18	50	<15	<2	2
F20-7H	23	65	19	48	<15	<2	<1
Glomeroporphyritic Gabbro							
B22-3	160	33	18	39	<15	<2	2
B22-8	29	57	16	48	<15	<2	<1
B23-15B	110	95	20	53	<15	<2	<1
B24-8A	185	86	20	378	<15	81	27
B32-3*	450	200	48	320	20	3	2
F12-10	164	24	14	16	<15	<2	17
F12-4	175	99	27	150	<15	5	7
F13-19A	96	41	19	87	<15	<2	<1
F13-3B	165	81	30	39	<15	9	1
F13-6A*		200		363	22	13	3
F14-1	75	23	23	38	<15	<2	<1
F14-12	600	74	21	44	<15	<2	4
F14-16	566	133	25	56	<15	<2	8
F14-18	880	139	24	52	<15	<2	8
F14-19	564	178	33	45	<15	10	3
F14-22	318	146	34	55	<15	12	1
F14-25	53	50	24	45	<15	<2	1
F14-28	405	39	20	46	<15	<2	2
F14-29*		425		450	<15	45	1
F14-3	187	40	21	15	<15	<2	<1
F14-31*		200		108	15	5	1
F14-33A	2345	486	84	17	29	78	24
F14-33B*		270		380	24	63	17
F14-38	187	85	26	93	34	16	1
F14-5	180	37	21	34	<15	<2	<1
F14-6	240	44	27	34	<15	<2	1
F14-8	194	46	23	39	<15	<2	<1
F16-1*		59		<10	5	27	1

Sample	Cu	Ni	Co	Cr	Pt	Pd	Au
F16-10	272	53	24	42	<15	<2	1
F16-11B	196	43	20	32	<15	<2	<1
F16-12	255	44	21	34	<15	<2	2
F16-14	326	44	29	50	<15	<2	4
F16-17	682	200	40	144	<15	16	7
F16-18	249	50	19	61	<15	<2	3
F16-19	352	74	25	139	<15	6	4
F16-2	535	88	35	42	<15	<2	<1
F16-21	200	49	23	100	<15	<2	<1
F16-4	160	30	21	26	<15	<2	2
F16-5	163	32	24	24	<15	<2	<1
F16-6	154	38	20	36	<15	<2	<1
F16-7	182	41	18	31	<15	<2	<1
F16-8*		141		82	230	7	2
F16-9	203	47	22	33	<15	<2	<1
F13-11	24	17	14	20	<15	<2	<1
F16-11A	30	23	16	48	<15	<2	<1
F22-10	72	121	27	57	<15	11	1
F22-4B	23	9	13	15	<15	<2	<1
F22-4C	13	24	16	32	<15	<2	<1
F22-5A	3	<15	11	128	<15	<2	<1
F22-5B	21	8	45	32	<15	<2	<1
F23-14	367	51	40	39	<15	<2	<1
F23-29	151	59	33	38	<15	<2	2
F23-40	58	20	14	36	<15	<2	<1
F26-1AA	88	57	24	144	<15	<2	<1
F871-6	193	38	27	48	<15	<2	2
F872-2	483	123	26	85	<15	8	2
H2-5	1900	340	56	210	<15	3	13
H3-1	280	79	51	80	<15	<2	2
H3-4	950	340	57	440	10	11	3
W24-12	124	35	17	34	<15	<2	<1
W24-13	16	35	10	14	<15	<2	<1
W24-6	330	<2	47	<2	<15	<2	<1
W24-8	246	65	52	70	<15	<2	3
W25-13	1410	525	61	125	16	66	177
W26-7	25	30	17	123	<15	<2	12
W29-5	342	71	25	89	<15	5	3
Normal Gabbro							
B22-9	107	14	18	179	<15	6	1
B23-1	118	95	25	133	<15	5	6
B23-11	162	76	24	60	<15	8	1
B23-3	97	28	41	69	<15	<2	10
B23-3A	94	32	35	72	<15	<2	18
B24-11	3	5	28	80	<15	<2	<1
B24-18	101	192	38	57	<15	11	2
B24-19	15	71	20	58	<15	5	3
B24-8B*		545		262	14	14	22
B25-1	62	37	21	54	<15	3	<1
B25-2	230	55	46	<2	<15	<2	<1

Sample	Cu	Ni	Co	Cr	Pt	Pd	Au
B31-5	1300	<2	82	0	<15	<2	9
F12-11	32	3	37	32	<15	<2	6
F12-14	3	4	15	55	<15	<2	<1
F12-13*		260		416	16	20	12
B23-15C	142	53	25	61	<15	<2	31
F12-16	13	<2	16	<2	<15	<2	<1
F13-8A	23	2	28	32	<15	<2	9
F13-8B	76	4	27	79	<15	<2	5
F18-12	163	26	29	44	<15	<2	<1
F18-14	82	14	29	52	<15	<2	<1
F18-21	25	67	29	252	<15	3	2
F18-4	50	95	28	81	<15	3	<1
F20-4	11	19	11	46	<15	<2	3
F22-12	244	33	19	54	<15	<2	<1
F22-14	98	36	22	51	<15	<2	<1
F22-16	130	76	21	141	15	9	2
F22-6	2	<2	3	91	<15	<2	<1
F22-7	3	<2	15	111	<15	<2	<1
F22-9	83	101	28	55	<15	11	<1
F23-15	15	<2	15	60	<15	<2	<1
F23-37	31	7	40	37	<15	<2	<1
F25-2	56	7	31	54	<15	<2	1
F25-3A	7	29	20	40	<15	<2	1
F25-3B	181	32	31	43	<15	<2	1
F25-7	72	145	28	66	<15	13	2
F876-9	258	42	19	116	<15	8	2
F876-1	177	41	23	48	<15	<2	5
F876-10	160	73	25	139	18	20	5
F876-12	140	81	33	124	21	27	5
F876-14	187	69	26	102	18	13	11
F876-16	205	65	26	79	<15	4	8
F876-3	204	37	23	54	<15	<2	<1
F876-5	186	30	22	42	<15	<2	2
F876-7	209	42	25	47	<15	<2	<1
H2-7	650	350	62	290	<15	16	4
H2-8	230	69	49	110	<15	2	2
H3-2	160	58	45	140	<15	2	<1
SH1-11	190	94	27	98	<15	3	5
SH1-2	79	69	26	138	<15	<2	<1
SH1-24	120	87	28	267	<15	6	3
SH1-28	130	68	24	518	<15	5	2
SH1-3	16	43	22	211	<15	<2	<1
SH1-32	104	75	24	80	<15	<2	5
SH1-35	198	84	25	132	<15	<2	6
SH1-38	194	112	33	166	<15	<2	<1
SH1-4	175	71	32	62	<15	3	2
SH1-41	191	65	26	53	<15	<2	<1
SH1-6	89	116	30	73	<15	9	3
SH1-8	80	84	23	52	<15	8	3
W24-11	29	119	22	151	<15	5	10

Sample	Cu	Ni	Co	Cr	Pt	Pd	Au
W24-11	29	119	22	151	<15	5	10
W24-14	170	90	29	332	<15	11	46
W25-10	11	4	14	76	<15	<2	1
W26-10B	9	102	21	37	<15	2	4
W26-15	130	252	36	94	<15	22	9
W26-5	168	105	21	123	<15	10	3
Metasediments							
B30-1	250	120	69	190	<15	7	3
B31-4	390	50	27	100	<15	3	2
F22-3A	64	21	20	29	<15	<2	<1
F872-3	507	32	39	157	<15	<2	<1
Pyroclastic							
HL-2					<5	5	2
HL-3					<5	2	2

Appendix B: Megascopic Descriptions

Howse Basalts

F18-25 Aphanitic massive basalt.
F20-9 Aphanitic massive basalt.
W29-2 Aphanitic massive basalt.

Anorthositic Gabbro

B30-2 Coarse grained anorthositic gabbro with minor hypersthene. Moderate alteration.
B31-1 Coarse grained anorthositic gabbro with 70% plagioclase. Moderate alteration.
B32-7 Coarse grained anorthositic gabbro with 75% plagioclase. Moderate alteration.
F13-3A 50% plagioclase aggregates in a medium-coarse grained gabbroic matrix containing minor bronzite. Low alteration.
F871-2 Extremely coarse grained anorthositic gabbro with interstices between plagioclase crystals filled by clinopyroxene and 10% iron-oxides.
F871-3 Extremely coarse grained anorthositic gabbro with 80% plagiclase and interstitial clinopyroxene and magnetite-ilmenite. Moderate alteration.
F871-4 Extremely coarse grained anorthositic gabbronorite with approximately 40% of the rock occupied by large plagioclase aggregates. Moderate alteration
F871-5 60% coarse plagioclase aggregates with interstitial clinopyroxene, minor plagioclase and 3% magnetite-ilmenite. Moderate alteration.
F872-1 Brecciated and disrupted anorthositic gabbro with very large plagioclase aggregates now silicified and albitized. Strong alteration.
H2-3 Coarse grained anorthositic gabbro with clinopyroxene and iron oxides interstitial to 65% plagioclase.
H2-6 35% very large plagioclase aggregates in a coarse grained subophitic gabbroic matrix. Moderate alteration.
H3-5 35% plagioclase aggregates in a matrix of coarse grained leucogabbro with minor bronzite. Low alteration.
W24-4 Extremely coarse grained anorthositic gabbro with 40% plagioclase aggregates which are almost indistinguishable from matrix crystals.
W25-7B Extremely coarse grained anorthositic gabbro with interstices between plagioclase crystals filled by clinopyroxene, iron oxides and quartz.
F20-7B 2% plagioclase phenocrysts and aggregates in a fine grained (chilled) matrix of subophitic gabbro. Moderate alteration.
F20-7H 40% plagioclase aggregates in a medium-coarse grained matrix of bronzite, clinopyroxene and iron oxides. Low alteration.

Glomeroporphyritic Gabbro

B22-3 Sparse plagioclase phenocrysts and aggregates in a medium grained matrix of ophitic gabbro. Low alteration.

B22-8 Sparse plagioclase aggregates in a fine grained (chilled) equigranular gabbro.

B23-15A Abundant, variably sized plagioclase aggregates form a framework to interstitial clinopyroxene, plagioclase, iron oxides and quartz.

B23-15B Sparse, small to very large plagioclase aggregates in a fine grained matrix of subophitic hypersthene-gabbro showing strong alteration.

B23-15C Strongly altered equigranular gabbro with 5-10% iron oxides.

B24-8A 5% plagioclase aggregates in a medium grained sub-ophitic gabbroic matrix containing minor hypersthene. Moderate alteration.

B31-2 Sparse plagioclase aggregates in a medium grained matrix of equigranular gabbro. Moderate alteration.

B31-3D1 Sparse plagioclase phenocrysts and aggregates in a medium grained gabbroic matrix. Strong alteration.

B32-3 Very sparse plagioclase phenocrysts and aggregates in a fine to medium grained matrix of equigranular gabbro with minor bronzite.

F12-10 Abundant plagioclase aggregates in a medium grained matrix of subophitic gabbronorite, with minor hypersthene. Intense alteration along fractures.

F12-13 Medium grained ophitic gabbro interlayered with glomeroporphyritic gabbro. Rock contains minor bronzite and shows moderate alteration.

F12-4 3-5% plagioclase phenocrysts and aggregates in a fine to medium grained matrix of subophitic mela-gabbronorite. Moderate alteration with quartz veins.

F13-19A 1-2 % small plagioclase phenocrysts or glomerocrysts in fine grained equigranular gabbro.

F13-3B 25% plagioclase aggregates in a medium grained matrix dominated by clinopyroxene and iron oxides, with minor radiating actinolite and 5% quartz pods.

F13-6A Sparse plagioclase aggregates in a medium grained matrix of ophitic olivine gabbro with minor secondary quartz. Moderate to strong alteration.

F14-1 3-5% plagioclase aggregates in a matrix of medium grained subophitic gabbro. Moderate alteration with aggregates showing strong epidotization.

F14-12 Sparse plagioclase aggregates set in medium grained ophitic gabbronorite with minor hypersthene. Fresh except in vicinity of quartz veining.

F14-16 3-5% plagioclase aggregates set in a matrix of medium grained hypersthene-gabbro. Rock shows moderately strong alteration.

F14-18 Abundant (5-10%) plagioclase aggregates set in a matrix of medium grained gabbronorite. Aggregates and matrix show low to moderate alteration.

F14-19 Very sparse fine plagioclase aggregates set in a matrix of medium grained gabbronorite. Rock shows low degree of alteration.

F14-22 Sparse plagioclase aggregates in a matrix of medium grained gabbronorite. Moderate alteration.

F14-25 Sample represents a vein within sparsely glomero-porphyritic gabbro. Gabbro has been completely replaced by albite, chlorite and actinolite.

F14-28 Abundant plagioclase aggregates in a matrix of medium grained ophitic gabbro with minor bronzite. Low alteration.

F14-29 Sparse plagioclase aggregates in a medium grained matrix of subophitic olivine melagabbro. Low alteration.

F14-3 2-3% small plagioclase aggregates set in a matrix of medium grained subophitic gabbro with minor hypersthene. Minor quartz-chlorite veins.

F14-31 Abundant plagioclase aggregates in a medium-coarse grained matrix of ophitic hypersthene-gabbro with 8-10% iron oxides. Moderate to strong alteration.

F14-33A Very sparse plagioclase aggregates in a matrix of medium grained gabbronorite with high sulphide content (12-15%) defining a stratiform horizon.

F14-33B Sparse plagioclase aggregates in a medium grained matrix of sub-ophitic gabbro. Elevated sulphide content defines stratiform horizon.

F14-38 Sparse plagioclase aggregates in a matrix of medium grained ophitic gabbronorite. Moderate alteration.

F14-5 Very sparse aggregates set in a matrix of medium grained subophitic gabbro with minor hypersthene.

F14-6 Very sparse plagioclase aggregates clots set in a matrix of medium grained subophitic hypersthene-gabbro.

F14-8 Very sparse plagioclase aggregates set in a matrix of medium grained ophitic gabbronorite. Low to moderate alteration.

F16-1 Very sparse plagioclase aggregates in a fine grained matrix of melagabbro with minor hypersthene and 10% iron oxides. Low alteration.

F16-10 Sparse small phenocrysts or aggregates of plagioclase set in a matrix of medium grained hypersthene gabbro. Moderate alteration.

F16-11B Host to vein of F16-11A. Sparse plagioclase aggregates in a matrix of medium grained ophitic hypersthene gabbro. Strong alteration near vein.

F16-12 Sparse plagioclase phenocrysts or aggregates set in a medium grained ophitic gabbro matrix containing minor hypersthene. Moderate alteration.

F16-14 Sparse plagioclase phenocrysts or aggregates set in a matrix of medium grained equigranular gabbro with minor hypersthene. Moderate alteration.

F16-17 Very sparse plagioclase aggregates in a matrix of medium grained ophitic gabbro. Low alteration.

F16-18 Very sparse plagioclase aggregates in a matrix of fine grained equigranular melagabbro. Low alteration.

F16-19 Sparse plagioclase aggregates and phenocrysts in a matrix of medium grained subophitic hypersthene-gabbro. Moderate alteration with minor chlorite pods.

F16-2 Very sparse plagioclase phenocrysts or aggregates in a matrix of medium grained melagabbro with minor hypersthene. Rock contains 10% magnetite.

F16-21 Abundant plagioclase aggregates in a matrix of medium grained, subophitic hypersthene gabbro. Moderate alteration with silicification.

F16-4 Sparse plagioclase aggregates in a matrix of medium grained subophitic, hypersthene-gabbro. Moderate alteration.

F16-5 Sparse plagioclase aggregates in a matrix of medium grained subophitic gabbro with minor hypersthene. Moderate alteration.

F16-6 Sparse plagioclase aggregates in a matrix of medium grained ophitic hypersthene gabbro. Rock contains 5% magnetite-ilmenite and shows vague lineation.

F16-7 Sparse plagioclase aggregates set in a matrix of medium grained gabbro with minor hypersthene. Rock is fresh.

F16-8 Very sparse plagioclase aggregates in a medium grained matrix of subophitic gabbro with minor hypersthene. Low alteration.

F16-9 Sparse, small plagioclase aggregates set in a matrix of medium grained sub-ophitic hypersthene-gabbro with 5(+)% magnetite, moderate alteration.

F22-10 10% plagioclase phenocrysts and glomerocrysts in a medium grained matrix of ophitic gabbronorite. Moderate alteration.

F22-4B 5% plagioclase aggregates in a medium grained matrix of subophitic gabbro. Strong alteration with quartz-chlorite filled fractures.

F22-4C Abundant plagioclase aggregates in a medium grained matrix of ophitic leucogabbronorite. Moderate to strong alteration.

F22-5A Strongly altered, fine to medium grained gabbro with abundant microfractures.

F22-5B Very sparse plagioclase phenocrysts in a sheared and completely altered, fine grained, gabbroic matrix.

F23-14 Very sparse plagioclase phenocrysts and aggregates in a medium grained matrix of melagabbro. Rock contains 15% iron oxides. Low alteration.

F23-29 Very sparse plagioclase phenocrysts and aggregates in medium grained equigranular melagabbro with 15-20% iron oxides. Low alteration.

F23-40 5% plagioclase phenocrysts and aggregates in medium grained matrix of equigranular leucogabbro. Moderate alteration.

F26-1AA Extremely large plagioclase aggregates form a framework to a medium grained matrix of equigranular gabbro with 5% quartz pods.

F871-6 Sparse plagioclase phenocrysts or aggregates in a matrix of fine to medium grained subophitic gabbro with minor hypersthene. Low alteration.

F872-2 Sparse plagioclase aggregates set in a matrix of medium grained gabbroic rock showing alternating plagioclase- and clinopyroxene-rich layers.

H2-5 Very sparse plagioclase phenocrysts and aggregates in a medium grained matrix of ophitic gabbro with minor hypersthene. Low alteration.

H3-1 2% plagioclase phenocrysts and aggregates in a fine to medium grained matrix of subophitic gabbro. Low alteration.

H3-4 5% plagioclase phenocrysts and aggregates in a medium grained equigranular gabbroic matrix. Low alteration.

W24-12 Very sparse plagioclase phenocrysts and aggregates in a matrix of medium grained subophitic gabbro with minor hypersthene. Low alteration.

W24-13 2% plagioclase phenocrysts and aggregates in a matrix of medium grained hypersthene-gabbro, with 5% iron oxides.

W24-8 2% plagioclase phenocrysts and aggregates in a matrix of equigranular gabbro showing strong alteration.

W25-13 5% plagioclase phenocrysts and glomerocrysts in a matrix of medium grained ophitic hypersthene melagabbro. Low alteration.

W26-7 Sparse plagioclase phenocrysts and glomerocrysts in a matrix of medium grained gabbro. Low alteration

W29-5 Rare plagioclase phenocrysts in a matrix of fine grained equigranular gabbro. Low alteration.

F13-11 Completely altered gabbro forming conformable, 1m thick zone. Alteration products include actinolite, chlorite, albite, chlorite and leucoxene.

F16-11A Sample represents a fracture zone in sparsely glomeroporphyritic gabbro. Vein consists of albite, quartz, actinolite, chlorite and clinopyroxene.

Normal Gabbro

B22-9 5% hypersthene phenocrysts set in a matrix of medium grained ophitic gabbro. Moderate to strong alteration.

B23-1 Medium grained equigranular to subophitic gabbro which has suffered intense quartz-chlorite veining.

B23-11 Medium grained subophitic gabbronorite showing moderate alteration.

B23-3	Medium grained equigranular to subophitic gabbro with moderately strong alteration.
B23-3A	Medium grained equigranular quartz-bearing gabbro showing strong alteration.
B24-11	Minor, completely serpentinized bronzite microphenocrysts in a medium grained matrix of equigranular gabbro. Strong alteration.
B24-18	3-5% plagioclase phenocrysts in a matrix of fine grained (chilled) gabbronorite. Moderate alteration.
B24-19	Very sparse plagioclase phenocrysts in a medium grained matrix of subophitic gabbronorite. Strong alteration.
B24-8B	Medium grained subophitic gabbro with elevated sulphide content.
B25-1	Medium grained ophitic gabbro with minor hypersthene. Moderate to strong alteration.
F12-11	Fine to medium grained hypersthene melagabbro with plagioclase laths in parallel orientation. Low alteration.
F12-14	Medium grained ophitic gabbro showing coarse prismatic clinopyroxene and mm-scale quartz nodules. Strong alteration.
F13-8A	Fine to medium grained subophitic gabbro with plagioclase in subparallel orientation. Low alteration.
F13-8B	Medium grained, highly altered gabbro showing mottled texture due to clustering of plagioclase in radiating patches with associated quartz.
F18-12	Moderately altered, medium-coarse grained, subophitic gabbro with minor quartz.
F18-14	Medium grained, equigranular melagabbronorite with 15% interstitial iron oxides.
F18-21	Fine grained, sheared and highly chloritized gabbro.
F18-4	Fine grained, highly altered, equigranular hypersthene gabbro with minor bronzite.
F20-4	Medium grained subophitic gabbro with minor carbonate. Moderate alteration.
F22-12	15% prismatic clinopyroxene microphenocrysts in a medium grained matrix of ophitic gabbronorite. Strong alteration with quartz-chlorite veins.
F22-14	20% prismatic to equant clinopyroxene microphenocrysts in a medium grained matrix of gabbronorite. Strong alteration.
F22-16	Medium grained equigranular to subophitic gabbro with minor bronzite. Moderate alteration with quartz-chlorite veins.
F22-6	Medium grained, subophitic diorite or quartz diorite. Moderate alteration.
F22-7	Rock consists of coarse prismatic clinopyroxene enclosed by a fine to medium grained intergrowth of plagioclase, quartz and leucoxene.

F22-9 Medium grained subophitic gabbronorite. Low alteration.

F23-15 Medium grained equigranular quartz gabbro with 5-10% leucoxene. Moderate to strong alteration.

F23-37 Fine grained equigranular gabbro. Strong alteration.

F25-2 Medium grained equigranular gabbro with 15% leucoxene and minor bronzite. Moderate alteration.

F25-3A Sample represents a pegamatitic zone with very coarse, prismatic clinopyroxene in a matrix of coarse ophitic gabbro. Moderate alteration.

F25-3B Medium grained subophitic gabbro. Moderate to strong alteration.

F25-7 3% plagioclase phenocrysts in a medium grained matrix of equigranular gabbronorite. Moderate alteration.

F876-9 Moderately altered, fine grained, chilled gabbro. Abundant microfractures.

F876-1 2-5% serpentinized hypersthene microphenocrysts in a matrix of medium grained subophitic gabbro. Minor alteration.

F876-10 Fine to medium grained partially chilled equigranular gabbro with occasional bronzite microphenocrysts. Moderately strong alteration.

F876-12 Medium grained equigranular gabbro with minor bronzite. Minor alteration.

F876-14 Medium grained equigranular gabbro with minor hypersthene. Low alteration with occasional quartz filled microfractures.

F876-16 Medium grained subophitic gabbronorite with minor hypersthene. Minor alteration with occasional microfractures.

F876-3 10% serpentinized hypersthene microphenocrysts set in a medium grained matrix of ophitic gabbro. Low to moderate alteration.

F876-5 3-5% serpentinized hypersthene microphenocrysts set in a medium grained matrix of ophitic gabbro. Moderate to strong alteration.

F876-7 5-8% serpentinized hypersthene microphenocrysts in a medium grained matrix of ophitic gabbro. Moderately strong alteration.

H2-7 Medium grained, subophitic to ophitic gabbro with minor bronzite. Moderate alteration.

H2-8 Medium grained ophitic gabbro showing moderate to strong alteration.

H3-2 Medium grained ophitic gabbro. Moderate to strong alteration.

SH1-11 Sparse (1%) plagioclase phenocrysts in mottled gabbronorite matrix with highly altered bronzite microphenocrysts.

SH1-2 Fine grained, chilled gabbro. Dense and massive with low degree of alteration.

SH1-24 Very sparse plagioclase phenocrysts in a medium grained subophitic gabbronorite matrix with 5% hypersthene. Low to moderate alteration.
SH1-28 Medium grained subophitic gabbronorite with minor hypersthene. Moderate alteration and minor quartz filled microfractures.
SH1-3 Fine grained, subophitic melagabbro with minor alteration.
SH1-32 Medium grained ophitic bronzite gabbro with minor hypersthene. Rock is mottled due to zones of extreme chloritization. Alteration moderate to strong.
SH1-35 Medium grained equigranular to subophitic gabbro with minor hypersthene. Moderate to strong alteration.
SH1-38 10% serpentinized hypersthene microphenocrysts set in a matrix of subophitic to ophitic gabbro containing minor bronzite. Strong alteration.
SH1-4 Fine to medium grained subophitic, bronzite microphyric melagabbronorite, with moderate alteration.
SH1-41 Medium grained subophitic gabbro with minor hypersthene. Moderate to strong alteration.
SH1-6 5 to 10% bronzite microphenocrysts in medium grained equigranular gabbronorite. Moderate alteration.
SH1-8 Medium grained equigranular gabbronorite with 5% hypersthene, and showing moderate alteration.
W24-11 Medium grained ophitic quartz gabbro with mottled texture resulting from radiating patches of plagioclase crystals. Strong alteration.
W24-14 Highly altered medium grained subophitic hypersthene gabbro with 15% iron oxides replaced by leucoxene.
W25-10 Highly altered, subophitic quartz gabbro.
W26-10B Strongly altered hypersthene gabbro, minor quartz veining.
W26-15 Highly altered and brecciated gabbro. Abundant quartz-chlorite veins and microfractures.
W26-5 Medium grained subophitic leucogabbro with minor bronzite. Low alteration.

Metasediments

B30-1 Finely laminated black shale.
B31-4 Laminated shale with minor quartzite layers.
F22-3A Well laminated, recrystallized argillite with minor quartzite lenses.
F872-3 Finely laminated, recrystallized and porphyroblastic argillite with cm-sized quartzite beds.

Pyroclastic Rocks

HL-2 Very fine grained chloritic tuff.
HL-3 Fine grained mafic tuff with vitric shards in a chloritic matrix.

Appendix C: Rare Earth Element Analyses

Rare-earth element analyses by neutron activation analysis at Ecole Poytechnique, Montreal. Concentrations are reported in ppm.

Sample	B23-5A	F13-19A	F20-7B	F20-9	F876-10	F8722-15
La	21.6	5.8	4.2	41.3	2.8	5.0
Ce	57.7	15.0	10.4	92.1	6.5	12.8
Nd	35.6	10.9	8.0	52.8	6.0	10.1
Sm	9.9	3.5	2.8	11.3	2.1	3.5
Eu	2.28	1.13	1.04	3.46	0.79	1.21
Tb	1.52	0.85	0.67	1.33	0.53	0.84
Dy	7.9	5.3	4.3	6.3	3.3	5.1
Ho	1.25	0.95	0.87	1.07	0.76	1.12
Yb	2.8	3.0	2.4	1.8	2.1	3.2
Lu	0.41	0.48	0.40	0.28	0.32	0.48

Sample	F8733-17	F8735-6	SH1-2	W29-2
La	5.1	5.4	3.1	33.3
Ce	13.0	15.0	8.9	78.2
Nd	11.5	11.5	6.3	47.4
Sm	3.6	3.8	2.6	10.6
Eu	1.04	1.25	0.71	3.89
Tb	0.87	0.88	0.68	1.28
Dy	5.5	5.7	4.4	6.0
Ho	1.19	1.31	1.04	1.05
Yb	3.1	3.3	2.7	1.8
Lu	0.46	0.53	0.41	0.26

B23-5A, F20-9, W29-2: Howse Lake basalts
F8722-15, F8733-17, F8735-6: Willbob Formation basalts
F13-19A Chilled glomeroporphyritic gabbro
F20-7B Chilled annorthositic gabbro
SH1-2, F876-10: Chilled normal gabbro

Appendix D: Whole Rock Analyses

Whole rock major and trace element data were obtained by X-ray fluorescence at the University of Ottawa. FeO was determined by wet chemical methods also at the University of Ottawa. Major element concentrations are reported in weight % oxides and trace element concentrations in ppm.

Appendix D: Glomeroporphyritic Gabbro Analyses

	B23-15B	B24-8A	B30-3	B31-2	B31-3	B32-3	F12-13	F13-19A
SIO2	48.00	46.80	48.60	48.10	48.30	46.70	46.27	49.32
TIO2	1.29	1.01	1.19	1.33	1.44	0.56	0.57	1.47
AL2O3	16.70	16.10	14.20	14.30	14.00	19.60	17.13	13.99
FE2O3T	12.80	13.30	13.10	13.40	14.20	8.64	11.46	15.72
FE2O3	1.98	2.05	2.02	2.06	2.19	1.33	2.75	2.22
FEO	9.74	10.12	9.97	10.20	10.81	6.58	7.84	12.15
MGO	5.25	6.95	6.58	6.84	6.24	7.12	6.59	6.45
CAO	8.71	8.07	11.30	9.98	9.35	11.50	12.20	7.38
NA2O	3.28	2.98	2.03	2.10	2.49	1.98	1.84	3.22
K2O	1.18	0.18	0.17	0.27	0.32	0.27	0.17	0.92
P2O5	0.12	0.09	0.09	0.11	0.12	0.05	0.00	0.05
MNO	0.22	0.21	0.20	0.23	0.24	0.13	0.14	0.31
S	0.00	0.00	0.00	0.00	0.00	0.00	0.09	0.04
LOI	3.85	4.98	2.96	3.61	3.67	3.81	3.13	3.18
TOTAL	100.43	99.66	99.39	99.22	99.24	99.74	98.89	100.89
BA	280	100	70	80	100	60	87	177
CR	120	490	150	110	120	320	416	117
ZR	60	20	40	80	80	30	28	79
SR	180	70	90	120	15	160	104	132
RB	90	20	10	10	0	0	0	30
Y	10	20	30	20	30	0	14	34
NB	20	20	20	10	10	20	0	0
ZN	88	60	70	110	79	65	40	215
NI	65	120	110	150	97	200	260	60
V	0	0	0	0	0	0	222	454

	F13-6A	F14-1	F14-12	F14-16	F14-18	F14-19	F14-22	F14-25
SIO2	47.08	51.11	48.26	49.06	48.15	47.41	47.36	48.43
TIO2	0.54	0.70	0.63	0.48	0.60	0.78	0.64	0.68
AL2O3	20.78	17.97	18.22	20.76	19.96	19.92	20.20	20.45
FE2O3T	8.93	10.56	9.11	7.55	8.06	10.10	8.70	7.48
FE2O3	1.74	1.90	0.72	1.33	0.36	1.21	1.59	1.30
FEO	6.47	7.79	7.55	5.60	6.93	8.00	6.40	5.56
MGO	6.99	5.72	6.33	5.25	5.60	5.65	5.79	4.35
CAO	12.26	11.50	12.12	13.14	12.26	11.83	12.44	11.36
NA2O	1.62	2.42	2.34	2.12	1.97	2.03	2.19	3.62
K2O	0.25	0.24	0.20	0.09	0.21	0.14	0.09	0.01
P2O5	0.00	0.00	0.04	0.00	0.03	0.04	0.02	0.00
MNO	0.12	0.16	0.15	0.13	0.15	0.20	0.21	0.11
S	0.06	0.02	0.14	0.03	0.11	0.09	0.08	0.01
LOI	2.24	1.69	2.75	1.80	2.75	2.96	2.71	4.78
TOTAL	100.29	101.32	99.57	99.92	99.21	100.39	99.86	100.74
BA	32	74	96	96	98	90	102	55
CR	363	67	194	233	220	142	320	70
ZR	24	25	31	21	25	29	37	33
SR	125	114	132	138	148	141	143	13
RB	0	0	0	0	0	0	0	0
Y	15	16	16	12	13	18	15	15
NB	0	0	0	0	0	0	0	0
ZN	54	60	58	101	38	55	32	62
NI	200	23	74	110	143	166	111	38
V	178	269	235	210	209	260	210	240

Appendix D: Glomeroporphyritic Gabbro Analyses

	F14-26	F14-28	F14-29	F14-3	F14-31	F14-33A	F14-33B	F14-33C
SIO2	49.49	48.67	46.80	49.53	47.33	46.07	47.16	46.30
TIO2	0.74	0.63	0.69	0.92	0.59	0.97	0.82	0.91
AL2O3	19.43	18.17	14.88	15.69	20.83	13.86	14.34	14.00
FE2O3T	9.00	9.42	15.38	10.49	10.06	14.92	14.52	14.92
FE2O3	1.71	1.45	1.62	0.75	2.61	4.27	3.53	4.08
FEO	6.56	7.17	12.38	8.76	6.70	9.58	9.89	9.75
MGO	5.36	6.32	10.84	6.35	7.24	7.96	8.10	7.96
CAO	11.61	12.32	9.79	12.30	11.33	11.53	11.56	11.53
NA2O	2.51	2.18	1.49	2.35	1.89	1.57	1.57	1.51
K2O	0.35	0.13	0.09	0.16	0.07	0.07	0.07	0.07
P2O5	0.00	0.04	0.00	0.05	0.00	0.00	0.00	0.00
MNO	0.16	0.16	0.20	0.19	0.13	0.19	0.19	0.19
S	0.06	0.06	0.00	0.05	0.03	0.08	0.05	0.08
LOI	2.45	2.76	1.38	2.35	2.26	3.06	1.76	2.24
TOTAL	100.55	100.17	100.42	99.56	101.11	99.40	99.21	98.80
BA	115	85	38	64	44	33	57	0
CR	115	186	460	43	108	418	354	380
ZR	38	27	12	31	21	33	35	34
SR	176	119	85	111	120	76	75	74
RB	0	0	0	0	0	0	0	0
Y	19	14	29	20	15	21	21	19
NB	0	0	35	0	0	0	0	0
ZN	49	73	120	55	39	76	65	78
NI	58	28	830	43	124	261	215	270
V	259	253	285	387	201	364	324	354

	F14-36	F14-38	F14-5	F14-6	F14-8	F16-1	F16-10	F16-11B
SIO2	48.41	48.33	50.91	49.03	49.73	45.39	50.30	49.85
TIO2	0.58	0.79	0.81	0.79	0.75	1.91	0.81	0.85
AL2O3	15.41	17.62	16.34	16.07	17.08	12.49	16.37	16.76
FE2O3T	12.55	10.31	10.74	10.37	9.39	19.39	9.92	9.92
FE2O3	2.25	1.49	2.32	1.60	1.37	6.74	1.21	1.28
FEO	9.27	7.94	7.58	7.89	7.22	11.38	7.84	7.77
MGO	8.17	7.70	6.28	6.80	6.40	6.76	6.13	6.17
CAO	11.94	11.83	12.42	11.79	12.54	11.65	12.41	12.43
NA2O	1.68	1.91	2.30	1.92	2.02	1.83	2.45	2.25
K2O	0.11	0.13	0.17	0.11	0.09	0.08	0.20	0.13
P2O5	0.00	0.06	0.00	0.06	0.06	0.00	0.05	0.03
MNO	0.17	0.16	0.18	0.17	0.17	0.19	0.29	0.19
S	0.23	0.03	0.02	0.06	0.09	0.02	0.05	0.09
LOI	2.30	3.10	2.06	2.58	2.44	1.59	2.39	2.19
TOTAL	100.75	101.23	101.49	98.98	100.07	100.30	100.62	100.11
BA	70	67	55	79	60	16	66	37
CR	522	298	61	124	133	0	146	102
ZR	28	41	35	38	38	30	40	36
SR	85	107	109	112	106	87	117	117
RB	0	0	0	0	0	0	0	0
Y	17	15	21	21	19	18	20	15
NB	0	0	0	0	0	0	0	0
ZN	61	60	43	47	49	65	67	122
NI	518	108	43	50	38	59	44	44
V	296	277	327	288	283	1341	320	306

Appendix D: Glomeroporphyritic Gabbro Analyses

	F16-12	F16-14	F16-17	F16-18	F16-19	F16-2	F16-21	F16-4
SIO2	49.73	49.03	47.90	49.65	48.92	43.64	49.19	49.81
TIO2	0.82	0.65	0.78	0.53	0.76	2.20	1.23	0.78
AL2O3	17.76	18.35	15.16	14.63	15.14	12.47	14.82	16.30
FE2O3T	9.82	9.33	11.89	10.82	11.16	21.57	13.57	10.46
FE2O3	1.52	1.44	2.34	1.15	1.59	3.32	1.35	0.31
FEO	7.47	7.10	8.59	8.70	8.61	16.42	11.00	9.13
MGO	5.76	5.80	8.45	9.80	8.41	6.55	6.65	6.04
CAO	12.18	12.91	11.56	12.02	11.84	11.10	10.73	12.08
NA2O	2.43	2.21	1.45	1.74	2.05	2.06	2.18	2.17
K2O	0.21	0.16	0.11	0.04	0.17	0.14	0.36	0.10
P2O5	0.05	0.04	0.01	0.02	0.03	0.02	0.00	0.00
MNO	0.19	0.15	0.24	0.20	0.20	0.19	0.22	0.17
S	0.07	0.14	0.05	0.05	0.12	0.04	0.04	0.09
LOI	2.53	1.81	3.42	1.57	2.47	1.83	2.82	2.23
TOTAL	100.84	99.92	100.22	100.22	100.47	100.34	100.75	99.30
BA	88	108	64	83	88	0	123	47
CR	141	241	394	272	398	0	199	25
ZR	32	26	20	14	26	36	60	34
SR	135	116	100	80	94	95	143	111
RB	0	0	0	0	0	0	0	0
Y	16	19	16	12	15	34	27	16
NB	0	0	0	0	0	40	0	0
ZN	67	62	36	65	57	102	59	113
NI	52	64	179	50	100	130	76	39
V	311	286	307	261	338	1694	412	260

	F16-5	F16-6	F16-7	F16-8	F16-9	F20-7B	F23-40	F26-1AA
SIO2	51.13	49.90	49.73	50.80	50.33	50.03	47.40	48.73
TIO2	0.82	0.85	0.88	0.78	0.78	1.22	0.61	1.28
AL2O3	16.06	15.52	15.61	16.61	16.32	14.23	20.70	14.13
FE2O3T	10.60	11.51	10.90	10.33	10.14	13.74	7.25	13.69
FE2O3	1.66	1.47	0.65	1.97	1.42	0.47	1.12	2.11
FEO	8.04	9.03	9.22	7.52	7.85	11.94	5.52	10.42
MGO	6.17	6.59	6.52	6.22	6.46	7.16	4.76	7.28
CAO	12.43	10.72	11.48	11.73	12.36	10.22	11.60	10.90
NA2O	2.28	3.34	2.51	2.43	2.68	2.20	3.24	2.22
K2O	0.10	0.29	0.35	0.23	0.20	0.39	0.48	0.15
P2O5	0.00	0.06	0.04	0.00	0.10	0.00	0.05	0.09
MNO	0.17	0.19	0.19	0.18	0.16	0.24	0.12	0.23
S	0.03	0.05	0.10	0.06	0.13	0.01	0.00	0.04
LOI	1.90	3.00	2.66	2.37	2.08	2.37	4.15	2.99
TOTAL	100.89	101.12	100.05	101.02	100.97	100.63	99.82	100.73
BA	46	107	75	82	60	118	80	58
CR	42	40	40	82	111	121	90	282
ZR	35	36	38	40	34	61	0	53
SR	107	136	135	134	107	103	190	103
RB	0	0	0	0	0	0	10	0
Y	19	20	15	20	18	26	20	33
NB	0	0	0	0	0	0	20	0
ZN	47	57	82	50	28	149	77	69
NI	35	32	50	141	45	58	34	78
V	314	338	336	307	296	376	0	393

Appendix D: Glomeroporphyritic Gabbro Analyses

	F871-6	F873-1	F873-4	H2-5	H3-1	H3-4	W24-12	W24-13
SIO2	49.85	47.51	49.36	47.90	49.70	46.60	49.30	48.80
TIO2	1.54	1.29	1.18	0.56	0.86	0.45	0.83	0.57
AL203	13.25	15.26	15.44	20.10	16.20	17.00	16.30	21.80
FE203T	14.93	14.63	12.60	9.10	10.70	10.20	10.50	6.53
FE203	1.19	1.56	1.94	1.40	1.65	1.58	1.62	1.01
FEO	12.36	11.76	9.59	6.93	8.14	7.76	7.99	4.97
MGO	6.13	7.02	6.63	6.00	6.12	8.47	6.09	3.78
CAO	9.42	6.14	11.32	11.80	11.30	11.80	10.70	12.40
NA20	2.79	3.85	2.04	1.81	2.33	1.57	2.86	2.97
K20	0.38	0.69	0.50	0.12	0.32	0.15	0.48	0.73
P205	0.11	0.09	0.07	0.06	0.07	0.03	0.06	0.05
MNO	0.24	0.26	0.19	0.12	0.18	0.14	0.19	0.12
S	0.02	0.07	0.09	0.00	0.00	0.00	0.00	0.00
LOI	3.31	4.40	2.21	2.62	3.07	3.56	3.36	2.55
TOTAL	100.76	100.09	100.71	99.53	100.01	99.25	99.85	99.81
BA	56	348	66	70	100	70	140	80
CR	84	184	194	210	80	440	60	40
ZR	70	70	70	20	20	10	20	20
SR	139	132	139	150	140	140	140	230
RB	0	0	0	0	0	0	30	50
Y	32	31	24	0	10	10	10	0
NB	0	0	0	10	30	0	30	10
ZN	237	148	114	65	68	73	96	41
NI	40	93	85	340	79	340	55	25
V	485	370	353	0	0	0	0	0

	W24-6	F16-11A
SIO2	45.90	66.71
TIO2	0.48	0.88
AL203	21.10	12.67
FE203T	8.47	4.63
FE203	1.30	0.65
FEO	6.45	3.58
MGO	7.56	1.97
CAO	12.10	5.99
NA20	1.75	3.87
K20	0.23	0.16
P205	0.05	0.24
MNO	0.11	0.11
S	0.00	0.04
LOI	2.42	2.11
TOTAL	99.56	99.08
BA	70	47
CR	320	24
ZR	0	307
SR	130	77
RB	10	0
Y	0	59
NB	20	15
ZN	50	161
NI	220	16
V	0	46

Appendix D: Normal Gabbro Analyses

	B22-9	B23-11	B24-8B	B25-1	B25-2	B31-5	F12-16	F22-6
SIO2	46.20	47.60	43.08	49.30	48.90	47.30	59.20	66.60
TIO2	0.76	1.03	0.96	1.35	0.96	0.57	0.63	0.72
AL2O3	19.90	14.00	12.04	13.00	16.20	14.40	15.10	11.20
FE2O3T	8.66	14.00	19.01	14.00	11.40	13.60	8.91	10.10
FE2O3	1.46	2.36	5.74	2.36	1.93	2.30	3.91	1.71
FEO	6.48	10.47	11.94	10.47	8.52	10.17	4.50	7.55
MGO	6.15	8.21	6.31	6.54	5.86	8.62	1.31	3.15
CAO	10.10	10.00	9.69	9.60	11.50	11.00	2.79	0.65
NA2O	2.55	1.92	1.61	2.45	1.96	1.37	5.30	3.17
K2O	1.32	0.60	0.17	0.63	0.25	0.14	3.01	1.30
P2O5	0.08	0.08	0.00	0.11	0.08	0.05	0.09	0.12
MNO	0.17	0.20	0.22	0.21	0.18	0.22	0.20	0.11
S	0.00	0.00	1.27	0.00	0.00	0.00	0.00	0.00
LOI	4.26	3.56	4.59	3.48	3.26	3.13	3.12	3.46
TOTAL	99.57	100.14	97.83	99.59	99.66	99.42	99.45	99.89
BA	240	230	114	110	70	80	1230	300
CR	360	180	262	200	90	530	40	40
ZR	40	40	48	70	40	0	620	500
SR	200	80	93	110	150	70	210	40
RB	70	20	0	40	30	0	80	70
Y	0	30	25	10	20	0	40	110
NB	20	20	0	10	0	10	110	40
ZN	48	70	71	58	64	90	100	83
NI	110	180	545	68	55	370	0	0
V	0	0	342	0	0	0	0	0

	F5-10	F876-9	F876-1	F876-10	F876-12	F876-14	F876-16	F876-3
SIO2	48.26	49.28	49.06	48.79	47.86	48.96	48.61	49.49
TIO2	1.10	1.01	0.73	0.96	0.90	0.85	0.84	0.77
AL2O3	13.86	12.54	17.26	13.80	14.72	14.56	15.23	16.48
FE2O3T	13.92	13.13	9.40	12.52	11.87	11.43	11.35	10.56
FE2O3	2.53	2.22	1.82	0.54	2.00	1.71	1.77	0.50
FEO	10.25	9.82	6.82	10.78	8.88	8.75	8.62	9.05
MGO	8.05	7.01	6.65	8.27	8.08	8.17	7.52	6.92
CAO	9.54	8.68	11.85	10.05	11.36	11.92	11.97	10.88
NA2O	2.19	3.74	1.93	1.95	2.07	2.03	2.14	2.74
K2O	0.27	0.39	0.48	0.97	0.68	0.36	0.40	0.65
P2O5	0.00	0.08	0.03	0.05	0.06	0.05	0.06	0.06
MNO	0.23	0.24	0.17	0.22	0.20	0.17	0.18	0.19
S	0.05	0.03	0.03	0.04	0.07	0.09	0.05	0.09
LOI	3.34	4.23	2.61	3.19	3.43	2.52	2.86	3.04
TOTAL	99.83	99.42	99.57	99.80	100.49	100.29	100.38	100.99
BA	202	150	125	205	119	66	76	165
CR	177	174	175	321	312	307	226	141
ZR	52	46	34	46	37	40	38	34
SR	110	80	162	158	185	122	104	181
RB	0	50	0	21	12	0	0	0
Y	28	22	19	24	20	21	21	17
NB	0	0	0	0	0	0	0	0
ZN	74	73	47	156	151	78	29	63
NI	90	62	39	99	102	102	83	46
V	399	348	280	347	317	316	324	281

Appendix D: Normal Gabbro Analyses

	F876-5	F876-7	H2-7	H2-8	H3-2	SH1-11	SH1-16	SH1-2
SIO2	49.36	49.34	45.50	49.30	49.50	48.08	46.86	49.42
TIO2	0.82	1.07	0.66	0.80	0.68	0.95	0.76	1.29
AL2O3	18.13	14.81	18.00	15.70	18.20	14.69	16.31	13.83
FE2O3T	10.18	12.95	10.40	10.50	8.83	13.88	11.98	14.71
FE2O3	1.72	2.19	1.75	1.78	1.50	1.98	1.78	1.70
FEO	7.61	9.68	7.78	7.85	6.60	10.71	9.18	11.71
MGO	5.72	7.15	8.79	6.61	5.80	8.93	9.92	7.63
CAO	10.40	8.84	11.00	11.30	10.80	10.53	10.40	6.63
NA2O	2.49	2.97	1.43	2.17	3.03	2.01	1.66	3.99
K2O	0.80	0.70	0.17	0.41	0.25	0.23	0.30	0.66
P2O5	0.03	0.08	0.06	0.07	0.06	0.08	0.04	0.11
MNO	0.19	0.25	0.19	0.17	0.14	0.20	0.20	0.27
S	0.04	0.08	0.00	0.00	0.00	0.05	0.06	0.03
LOI	2.92	3.39	4.03	3.10	3.50	2.40	2.80	3.89
TOTAL	100.37	100.70	99.49	99.32	100.13	100.98	100.43	101.33
BA	198	223	90	80	100	67	75	188
CR	84	85	290	110	140	183	141	201
ZR	41	45	0	10	20	39	37	59
SR	221	141	110	110	120	86	160	117
RB	16	12	0	0	20	0	0	0
Y	22	24	10	0	10	25	19	30
NB	0	0	20	30	20	0	0	0
ZN	125	76	120	62	41	68	222	73
NI	37	39	350	69	58	135	266	69
V	290	376	0	0	0	323	231	448

	SH1-22	SH1-24	SH1-28	SH1-3	SH1-32	SH1-35	SH1-38	SH1-4
SIO2	46.61	47.73	47.96	48.93	50.08	48.08	48.18	49.08
TIO2	0.64	0.57	0.65	1.27	0.90	0.57	0.77	1.14
AL2O3	15.13	18.08	16.71	13.42	15.75	17.07	13.02	14.02
FE2O3T	12.82	8.48	9.09	16.15	9.96	8.47	11.38	13.48
FE2O3	2.30	1.01	1.53	2.73	1.52	1.44	2.38	1.02
FEO	9.47	6.72	6.80	12.08	7.59	6.33	8.10	11.21
MGO	12.62	7.67	8.01	7.44	7.20	8.33	10.34	7.77
CAO	9.54	12.96	10.70	6.33	11.27	13.28	12.31	10.78
NA2O	1.44	2.10	2.52	3.12	2.69	1.81	1.52	2.36
K2O	0.18	0.33	0.76	0.35	0.20	0.30	0.10	0.29
P2O5	0.01	0.04	0.06	0.05	0.23	0.05	0.03	0.07
MNO	0.20	0.14	0.18	0.27	0.15	0.16	0.19	0.20
S	0.06	0.00	0.05	0.04	0.05	0.09	0.07	0.06
LOI	2.99	3.05	3.19	4.15	3.16	2.71	3.12	2.56
TOTAL	101.33	100.58	99.36	100.35	100.93	100.38	100.29	100.71
BA	58	86	243	197	41	156	86	90
CR	153	572	692	202	260	372	356	183
ZR	33	24	30	58	157	23	25	49
SR	101	138	153	94	116	181	90	96
RB	0	0	24	0	0	0	0	0
Y	16	13	17	24	45	12	16	25
NB	0	0	0	0	0	0	0	0
ZN	80	55	170	69	89	50	44	85
NI	359	113	98	46	95	115	149	88
V	195	228	275	451	186	229	334	403

Appendix D: Normal Gabbro Analyses

	SH1-41	SH1-6	SH1-8
SIO2	49.06	47.91	48.23
TIO2	0.63	1.01	0.98
AL2O3	17.79	14.12	14.14
FE2O3T	8.92	12.72	13.74
FE2O3	1.95	2.15	2.33
FEO	6.27	9.51	10.27
MGO	7.07	8.88	9.01
CAO	13.00	10.12	11.06
NA2O	2.35	2.18	2.18
K2O	0.21	0.59	0.24
P2O5	0.04	0.06	0.07
MNO	0.15	0.26	0.20
S	0.05	0.05	0.06
LOI	2.54	3.38	2.42
TOTAL	101.24	100.38	101.33
BA	83	115	81
CR	215	179	163
ZR	30	50	44
SR	160	106	85
RB	0	16	0
Y	15	23	20
NB	0	0	0
ZN	54	64	89
NI	82	155	151
V	257	361	354

Appendix D: Anorthositic Gabbro Analyses

	B30-2	B30-2A	B31-1	B32-7	F16-20	F871-3	F871-4	F871-5
SIO2	48.00	49.20	47.50	47.30	45.79	47.43	46.94	48.24
TIO2	0.36	0.79	1.19	0.61	0.88	0.83	0.67	0.64
AL2O3	24.00	19.10	18.90	20.60	21.82	22.06	21.36	21.29
FE2O3T	5.73	8.98	10.30	8.15	10.46	11.01	8.46	8.42
FE2O3	0.81	1.27	1.45	1.15	0.94	1.57	0.45	1.21
FEO	4.43	6.94	7.96	6.30	8.57	8.49	7.21	6.49
MGO	2.78	5.07	4.48	6.22	5.52	4.13	5.63	4.81
CAO	14.20	11.40	10.10	12.70	8.61	6.98	12.73	12.39
NA2O	2.30	2.57	2.94	1.77	3.07	4.57	2.04	2.16
K2O	0.40	0.43	0.40	0.30	0.19	0.12	0.31	0.28
P2O5	0.06	0.07	0.09	0.06	0.01	0.03	0.06	0.02
MNO	0.10	0.17	0.18	0.12	0.14	0.12	0.11	0.12
S	0.00	0.00	0.00	0.00	0.06	0.05	0.03	0.09
LOI	3.03	3.08	4.36	2.63	2.63	4.74	2.90	4.47
TOTAL	100.53	100.17	99.64	99.87	98.41	101.23	100.54	102.33
BA	70	90	110	50	91	69	85	93
CR	70	150	80	350	410	119	125	144
ZR	0	40	70	0	34	20	29	29
SR	210	160	130	130	192	209	162	166
RB	30	20	10	10	0	0	0	0
Y	0	10	20	10	13	0	13	15
NB	10	20	20	20	0	0	0	0
ZN	55	51	170	54	96	0	35	116
NI	70	97	77	190	62	34	87	60
V	0	0	0	0	316	316	206	215

	F874-12	F874-17	F874-21	F874-6	F874-9	H2-2	H2-3	H2-4
SIO2	47.97	47.39	49.10	47.71	47.84	48.50	47.50	47.40
TIO2	0.62	0.86	0.40	0.89	0.69	0.80	0.72	0.49
AL2O3	21.77	23.19	23.63	20.32	21.64	20.60	21.40	24.80
FE2O3T	8.01	6.89	6.45	9.04	9.50	8.03	8.79	6.34
FE2O3	1.13	0.97	0.90	1.27	2.61	1.13	1.23	0.89
FEO	6.19	5.33	4.99	6.99	6.20	6.21	6.80	4.90
MGO	4.47	2.90	2.46	4.60	4.04	3.82	3.98	2.64
CAO	13.07	12.87	13.28	12.03	11.04	9.56	11.20	14.20
NA2O	1.95	2.22	2.48	2.31	3.01	3.89	2.35	1.94
K2O	0.24	0.29	0.27	0.64	0.41	0.35	0.90	0.25
P2O5	0.02	0.02	0.04	0.02	0.02	0.06	0.06	0.07
MNO	0.13	0.11	0.09	0.15	0.13	0.14	0.17	0.10
S	0.02	0.11	0.05	0.08	0.06	0.00	0.00	0.00
LOI	2.28	2.85	2.52	3.01	3.25	4.08	3.53	2.71
TOTAL	99.96	99.22	100.29	100.15	101.04	99.35	99.94	100.44
BA	47	78	96	97	84	130	330	40
CR	68	65	42	77	54	130	50	40
ZR	34	27	49	41	30	10	0	20
SR	201	259	209	246	231	180	260	230
RB	0	0	0	14	0	10	30	20
Y	11	10	23	15	10	20	0	0
NB	0	0	0	0	0	20	10	20
ZN	143	68	90	96	61	1100	79	0
NI	55	43	20	57	33	100	83	0
V	173	249	89	281	196	0	0	0

Appendix D: Anorthositic Gabbro Analyses

	H2-6	H3-5
SIO2	45.50	44.00
TIO2	0.51	1.00
AL2O3	19.40	18.60
FE2O3T	10.50	13.40
FE2O3	1.48	1.89
FEO	8.12	10.36
MGO	5.94	4.84
CAO	11.80	11.60
NA2O	1.39	1.26
K2O	0.25	0.13
P2O5	0.04	0.06
MNO	0.14	0.20
S	0.00	0.00
LOI	4.52	4.77
TOTAL	99.23	98.95
BA	110	100
CR	100	60
ZR	0	10
SR	170	150
RB	0	0
Y	0	0
NB	0	20
ZN	79	82
NI	640	1500
V	0	0

Appendix D: Le Fer Basalt Analyses

	B88-26	B88-30	B88-31	B88-36	B88-37	99419	99420	720
SIO2	49.55	47.95	49.50	49.04	49.29	48.70	46.40	48.00
TIO2	0.98	1.02	0.98	0.99	1.02	1.38	1.33	1.26
AL2O3	13.98	15.11	14.91	14.26	14.34	13.50	14.10	13.60
FE2O3T	12.59	13.76	12.78	12.07	12.51	13.50	14.70	13.90
FE2O3	1.97	1.70	1.67	1.46	1.66	1.79	1.95	1.84
FEO	9.56	10.85	10.00	9.55	9.76	10.54	11.47	10.85
MGO	7.22	8.48	7.72	7.44	7.50	6.79	7.42	8.08
CAO	12.41	9.80	10.04	11.81	11.89	10.10	8.78	5.80
NA2O	1.96	1.83	1.94	1.69	1.90	1.90	2.65	2.84
K2O	0.07	0.17	0.09	0.07	0.09	0.31	0.16	0.51
P2O5	0.05	0.05	0.05	0.04	0.05	0.11	0.10	0.10
MNO	0.21	0.21	0.18	0.20	0.20	0.20	0.20	0.22
S	0.05	0.06	0.12	0.13	0.11	0.00	0.00	0.00
LOI	3.04	4.19	3.39	2.57	2.60	3.89	4.59	7.50
TOTAL	101.20	101.58	100.74	99.41	100.56	99.40	99.32	100.73
BA	21	169	85	88	66	158	50	123
CR	263	243	229	268	260	270	290	0
ZR	51	53	55	51	48	87	83	83
SR	156	90	104	113	107	210	97	70
RB	0	0	0	0	0	11	5	15
Y	23	20	20	22	19	25	25	8
NB	0	0	0	0	0	3	0	0
ZN	151	102	92	93	94	76	83	106
NI	76	118	118	112	74	95	108	105
V	315	334	325	325	336	391	381	398

	721	722	723	724	718
SIO2	51.00	48.90	49.20	48.30	49.10
TIO2	1.13	1.29	1.20	1.20	1.43
AL2O3	13.60	13.90	14.00	13.70	14.30
FE2O3T	13.50	13.60	12.20	16.50	13.40
FE2O3	1.79	1.81	1.62	2.19	1.78
FEO	10.54	10.61	9.52	12.88	10.46
MGO	6.12	6.83	6.65	6.85	6.72
CAO	9.29	10.70	10.30	8.26	10.40
NA2O	3.41	2.00	1.85	1.13	1.98
K2O	0.07	0.65	0.17	0.15	0.42
P2O5	0.09	0.08	0.08	0.09	0.10
MNO	0.19	0.21	0.21	0.25	0.19
S	0.00	0.00	0.00	0.00	0.00
LOI	4.01	3.63	4.02	4.69	3.76
TOTAL	101.33	100.77	98.96	99.82	100.78
BA	26	208	77	46	118
CR	0	0	0	0	0
ZR	0	77	78	89	88
SR	0	230	130	130	160
RB	0	21	8	4	16
Y	0	25	25	25	27
NB	0	0	0	0	0
ZN	69	68	169	108	93
NI	112	102	107	106	93
V	359	383	374	355	380

Appendix D: Willbob Basalt Analyses

	F87-100	F8722-15	F8722-2	F8723-18	F8733-17	F8735-6	F8736-1
SIO2	48.06	48.95	49.44	47.66	49.66	48.81	48.68
TIO2	1.26	1.46	1.56	1.10	1.60	1.55	1.54
AL2O3	14.90	13.33	13.85	14.28	13.93	13.87	13.83
FE2O3T	13.05	14.16	14.93	12.72	14.89	14.70	14.44
FE2O3	2.16	2.84	3.64	2.56	3.07	2.96	3.22
FEO	9.80	10.19	10.16	9.14	10.64	10.56	10.10
MGO	8.25	5.76	6.22	8.47	6.59	6.14	5.98
CAO	8.84	12.06	10.42	10.68	8.71	10.12	10.61
NA2O	2.43	1.27	2.00	1.66	2.07	1.69	2.23
K2O	0.31	0.17	0.16	0.34	0.18	0.23	0.16
P2O5	0.09	0.14	0.14	0.09	0.14	0.13	0.12
MNO	0.20	0.21	0.21	0.20	0.21	0.20	0.20
S	0.01	0.08	0.00	0.10	0.02	0.08	0.06
LOI	3.89	3.34	3.08	3.49	3.56	3.30	2.90
TOTAL	100.34	99.94	101.04	99.92	100.53	99.78	99.78
BA	106	44	58	107	19	0	40
CR	107	113	113	214	124	114	115
ZR	63	76	80	55	86	80	82
SR	74	126	156	105	108	115	124
RB	0	0	0	0	0	0	0
Y	25	32	34	27	34	33	32
NB	0	0	0	0	0	0	0
ZN	121	80	101	83	80	76	93
NI	126	51	62	127	33	49	41
V	342	430	478	342	466	463	464

Appendix D: Howse Basalt Analyses

	B23-5B	F18-25	F18-26	F20-9	W29-2
SIO2	43.05	42.10	43.73	43.32	42.60
TIO2	4.75	4.84	4.56	5.06	5.43
AL2O3	12.31	13.60	13.62	12.79	12.60
FE2O3T	16.12	17.50	13.68	18.02	17.20
FE2O3	2.68	2.81	2.13	2.64	2.59
FEO	12.09	13.22	10.39	13.84	13.15
MGO	7.80	6.24	5.93	6.57	7.23
CAO	5.41	7.48	10.21	6.53	5.53
NA2O	1.93	2.92	3.40	2.91	2.49
K2O	1.89	0.61	0.91	1.53	2.13
P2O5	0.81	0.50	0.48	0.70	0.67
MNO	0.16	0.31	0.31	0.24	0.41
S	0.10	0.00	0.08	0.02	0.00
LOI	6.44	4.63	4.07	3.44	4.62
TOTAL	99.57	99.40	100.06	99.75	99.68
BA	317	340	336	325	1190
CR	0	90	18	0	30
ZR	187	180	160	177	180
SR	83	220	553	213	250
RB	18	20	14	32	50
Y	28	10	26	30	20
NB	39	50	27	38	60
ZN	293	150	300	89	120
NI	0	77	17	0	34
V	190	0	356	299	0

Appendix D: Tait Lake Gabbro Analyses

	B88-22	B88-24	B88-29	B88-32	B88-34	B88-40
SIO2	48.27	48.38	50.13	48.23	48.23	50.55
TIO2	0.71	0.60	1.05	1.28	1.17	1.17
AL2O3	14.62	15.75	12.50	13.86	14.49	14.29
FE2O3T	10.48	8.96	10.05	13.49	12.83	12.97
FE2O3	0.92	1.55	1.25	1.35	1.15	2.23
FEO	8.60	6.67	7.92	10.92	10.51	9.66
MGO	8.90	8.85	8.26	7.04	7.42	5.55
CAO	12.21	12.79	13.46	10.11	10.13	8.79
NA2O	1.42	2.21	2.26	1.99	2.66	2.86
K2O	0.53	0.20	0.07	0.16	0.22	1.52
P2O5	0.02	0.03	0.04	0.07	0.05	0.07
MNO	0.17	0.16	0.22	0.22	0.21	0.41
S	0.09	0.04	0.04	0.14	0.05	0.06
LOI	2.79	3.75	3.20	3.96	4.11	2.57
TOTAL	99.49	101.16	100.57	99.47	100.58	100.01
BA	98	93	72	54	131	1003
CR	783	585	339	212	259	18
ZR	34	59	56	60	54	60
SR	171	116	114	105	158	246
RB	0	0	0	0	0	27
Y	17	19	19	23	21	20
NB	0	0	0	0	0	0
ZN	214	126	137	78	141	488
NI	154	121	108	69	76	27
V	233	176	331	367	375	339